CALIFORNIA STATE UNIVERSITY, NORTHRIDGE

SOLITONS IN ^{4}HE SUPERFLUID

A thesis submitted in partial fulfillment of the requirements
for the degree of Master of Science
in Physics

By

David Levy

December 2018

Copyright by David Levy 2018

The thesis of David Levy is approved:

_____	_____
Jussi Eloranta, Ph.D.	Date
_____	_____
Yohannes Shiferaw, Ph.D.	Date
_____	_____
Miroslav Peric, Ph.D., Committee Chair	Date

California State University, Northridge

ACKNOWLEDGEMENTS

It is my pleasure to thank to Dr. Jussi Eloranta for his able supervision, support, and countless discussions on the subject that benefited this thesis. I would also like to thank Dr. Miroslav Peric for his invaluable support during my studies at California State University, Northridge. Finally, I would like to thank my Mother and the Levy Family for their support and encouragement.

Table of Contents

Signature page iii

Acknowledgements iv

List of figures vii

Abstract viii

1. Introduction Page | 1

1.1 Solitary waves: Historical background of solitons Page | 1

1.2 The Kdv Equation Page | 2

1.3 The Discovery of Solitons Page | 5

1.4 Shockwaves Page | 6

2. Theory of Solitons in ^{4}He Page | 8

2.1 The Gross- Pitaivski Equation a Non-Linear Schrodinger Equation Page | 8

2.2 Density Functional Theory for ^{4}He Systems Page | 11

3. Numerical Methods Page | 16

3.1 Numerical scheme and evaluation of energy Page | 16

3.2 Time-space discretization of DFT equation Page | 16

4. Experimental observations of solitons in Helium superfluid. Page | 19

4.1 Solitons in ultracold materials. Page | 19

4.2 Experimental Observations of solitons in bulk ^{4}He superfluid Page | 20

5. Discussion Page | 21

5.1 Numerical Result Page | 21

5.2 Shockwave Velocities Page | 22

5.3 Soliton Velocities Page | 24

5.4 Soliton Halfwidth Page | 26

5.5 Density Page | 28

5.6 Soliton Amplitude Page | 30

5.7 Soliton Final Result Page | 31

6. Conclusion Page | 32

6.1 Solitons in bulk ^{4}He superfluid Page | 32

References Page | 33

Appendix: Publication on Physical Review Letters Page | 35

List of Figures

1. Original figure from Scott Russel 'Report on waves' Page| 1
2. Breaking of an initial state into solitons Page| 6
3. Inner Potentials: OP, OT, BB Page| 13
4. Geometry of solid metal target immersed in bulk superfluid helium Page| 20
5. Shadowgraph snapshots of the waves emitted from the target Page| 20
6. Soliton and shockwave propagation simulation result Page| 21
7. Shockwave velocity for simulation 1 Page| 22
8. Shockwave velocity for simulation 2 Page| 23
9. Shockwave velocity for simulation 3 Page| 24
10. Soliton velocity of simulation 1 Page| 25
11. Soliton velocity of simulation 2 Page| 25
12. Soliton velocity of simulation 3 Page| 26
13. Halfwidth of soliton for simulation 1 Page| 27
14. Halfwidth of soliton for simulation 2 Page| 27
15. Halfwidth of soliton for simulation 3 Page| 28
16. Density-velocity for shockwaves Page| 29
17. Density-velocity for solitons Page| 29
18. Soliton Amplitude-Velocity Page| 30
19. Time evolution of the average soliton velocity at 1.7 K Page| 31

ABSTRACT

SOLITONS IN ^{4}HE SUPERFLUID

By

David Levy

Master of Science in Physics

In this thesis we study soliton wave simulations constructed in the context of the Gross-Pitaivski Equation, a form of the Non-Linear Schrodinger Equation (NLS), and Time-dependent density functional theory (TDDFT). The above simulations allow us to identify soliton wave solutions in bulk superfluid ^{4}He and study their dynamic properties. For the first time in the study of superfluid's, bright soliton where observed in bulk superfluid ^{4}He. Both experimental and numerical simulation results are presented. Several characteristics of bright soliton dynamics in bulk ^{4}He superfluid were observed and are investigated in this thesis.

1. Introduction

1.1 Solitary waves: Historical background of solitons

The first observation of solitary waves is recorded in history by John Scott Russel on the Edinburgh-Glasgow canal in 1843. In his 'Report on waves' reported to The British Association for the Advancement of Science in 1844, Russel describes these solitary waves as great waves of translation: "*I was observing the motion of a boat which was rapidly drawn along a narrow channel by a pair of horses, when the boat suddenly stopped - not so the mass of water in the channel which it had put in motion; it accumulated round the prow of the vessel in a state of violent agitation, then suddenly leaving it behind rolled forward with great velocity, assuming the form of a large solitary elevation, a rounded, smooth and well defined heap of water, which continued its course along the channel apparently without change of form or diminution of speed. I followed it on horseback, and overtook it still rolling on at a rate of some eight or nine miles an hour, preserving its original figure some thirty feet long and a foot to a foot and a half in height. Its height gradually diminished, and after a chase of one or two miles I lost it in the windings of the channel. Such, in the month of August 1834, was my first chance interview with that singular and beautiful phenomenon which I have called the Wave of Translation*." [1]

Russel subsequently performed many laboratory experiments. In these experiments he dropped a weight at one end of a water channel to generate solitary waves (see Fig. 1.1). Additionally, he was able to observe that the volume of the water in this wave is equal to the water displaced and further, the speed c which is measured in (m/s) of the above solitary wave is obtained as follows:

$$c^2 = g\,(h+a) \qquad (1.1)$$

where a is the amplitude measured in (m) of the wave, h is undisturbed height or depth of the water measured in (m) and g is the acceleration due to gravity. Thus, the waves produced in Russel's experiment are better described as 'Gravity waves'. [1]

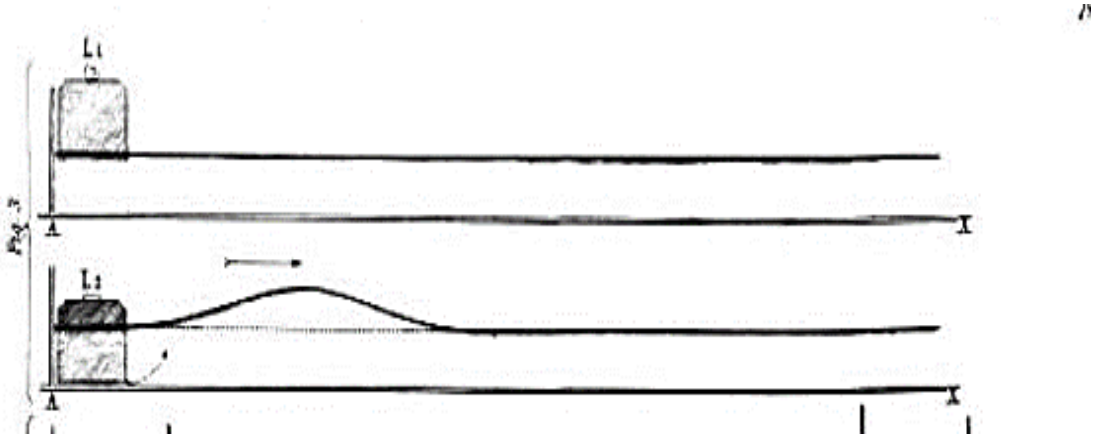

Fig 1.1: Original figure from Scott Russel 'Report on waves'[2]

Furthermore, based on equation (1.1) we can also deduce that higher amplitude waves would travel faster. We can also see that since equation (1.1) applies to waves of elevation, we cannot possibly generate by this method waves of dispersion. Instead, any attempt to generate waves of dispersion would result in a train of oscillatory waves. [1]

Although, at the time Russel made his discovery, contemporary theories on water waves did not support his findings and in general it was believed that water waves could not propagate without change in shape. Later research carried out in 1871 by Joseph Boussinesq and independently in 1876 by Lord Rayleigh confirmed that the effects of non-linearity and dispersion can balance each other out or more specifically that solitary waves self-reinforce as they propagate. This subtle yet counterintuitive discovery is what allows for solitary waves to propagate without change in shape. [1,3]

Russel's formula was further examined and expanded by both Boussinesq (1871) and later by Rayleigh (1876). In both cases the discovery they made from Russel's equation is that a solitary wave has a length scale much greater than the that of the depth of the water it traverses on. Moreover, they were also able to show that the wave depth profile $z = \zeta(x,t)$ is given by

$$\zeta(x,t) = a\,\mathrm{sech}^2\{\beta(x-ct)\} \qquad (1.2)$$

where $\beta^2 = 4h^2(h+2)/3a$ for any $a>0$ and the *sech* profile is correct only for $a/h << 1$. However, an equation for $\zeta(x, t)$ that admits equation (1.2) as a solution did not appear until 1895 in the form of the KdV (Korteweg & De Vries) equation.

1.2 The Kdv Equation

In this section I will illustrate how the *KdV* equation arises from the original fundamental equations for solitary waves discussed so far. I will also show the derivation of the standard *KdV* equation as considered by Korteweg & De Vries. [1] Although, Boussinesq is believed to have originally discovered the KdV equation, it was not well understood until 1895. In 1895 Korteweg & De Vries showed that the solution to the above solitary wave equation takes the form:

$$\frac{\partial \zeta}{\partial t} = \frac{3}{2}\left(\frac{g}{h}\right)^{1/2}\left(\frac{2}{3}\varepsilon\frac{\partial \zeta}{\partial \chi} + \zeta\frac{\partial \zeta}{\partial \chi} + \sigma\frac{\partial \zeta}{\partial \chi}\right) \qquad (1.3)$$

where χ is the coordinate moving with the wave, σ incorporates the surface tension parameter, T, which has the form $\sigma = {}^{1}/_{3}\, h^3 - {}^{Th}/_{g}\, \rho$, here ρ is the density of the liquid and ε is an arbitrary parameter. For convivence we can change variables as follows:

$$\zeta = \zeta(X,t) \qquad \textit{and} \qquad \chi = x + \varepsilon \left(\frac{g}{h}\right)^{1/2} t$$

We can now re-cast equation (1.3) in the form

$$\zeta_t = \frac{3}{2}\left(\frac{g}{h}\right)^{1/2} \left(\zeta\zeta_x + {}^{1}/_{3}\, \sigma\zeta_{xxx}\right) \qquad (1.4)$$

The above equation is a form of the *KdV* equation and admits equation (1.2) as a solution for ζ(x,t). [1]

In standard form or in the form originally considered by Korteweg & De Vries we can write the KdV equation as follows

$$u_t - 6uu_x + u_{xxx} = 0 \qquad (1.5)$$

The solutions for this traveling wave can be obtained by making the *ansatz u(x,t) = f(ζ)*, where *ζ = (c – xt)* and *c* is a constant. Thus, by substituting this into equation (1.5) we have the following equation:

$$-cf' - 6ff' + f''' = 0$$

Integrating this equation yields

$$-cf - 3f^2 + f'' = A$$

where *A* is a constant of integration. We can now choose f'' as integrating factor and by integrating for a second time we have the following equation:

$$\frac{1}{2}(f')^2 = f^3 + \frac{1}{2}cf^2 + Af + B$$

where *B* is a second constant of integration. If we now impose boundary conditions as follows $f,\ f'', f'' \to 0\ , as\ \zeta \to \pm\infty$. We can see that the above conditions describe a *solitary wave*. Thus, both *A* and *B* are zero and,

$$(f')^2 = f^2(2f + c)$$

from this we can also see that a real solution exits only if $(f')^2 \geq 0$ or we we can say that $2f + c \geq 0$.

We can integrate the above equation in the following way

$$\int \frac{df}{f(2f + c)} = \pm \int d\zeta$$

Here we can use the substitution $f = -\frac{1}{2} c \, sec\, h^2\theta$ $(c \geq 0)$ to obtain

$$f(x - ct) = -\frac{1}{2} \sec h^2 \left\{ \frac{1}{2} c^{\frac{1}{2}} (x - ct - x_0) \right\} \qquad (1.6)$$

where x_0 is arbitrary constant of integration. An interesting detail is that this solution is an even function, so we may disregard the $\pm$ above. We can also see that x_0 tells us the phase shift or more precisely denotes the position of the peak at *t = 0*. Equation (1.6) is a solution for a solitary wave and can also be written for simplicity as follows. Taking *u(x , t) = f(x - ct)* we arrive at our final solution for the KdV equation:

$$u(x, t) = -\frac{1}{2} \sec h^2 \left\{ \frac{1}{2} c^{\frac{1}{2}} (x - ct - x_0) \right\} \qquad (1.7)$$

1.3 The Discovery of Solitons

Solitons can be best described as self-reinforcing non-dissipative solitary waves that maintain their speed and shape upon collision with other such waves. Solitons are produced by the cancelation of non-linear effects in a medium. In the previous section I illustrated how the *KdV* equation arises from the original fundamental equations for solitary waves. It is interesting to note that the KdV Equation we studied in our previous section is related to the Klein Gordon (KG) equation $u_{xx} - u_{tt} = u$ which was discovered by Physicists Oskar Klein and Walter Gordon in 1926 and greatly added to our understanding of solitary waves. Later in history in the 1950's Physicist Martin David Kruskal coined the term Sine-Gordon equation as a pun on the name of the Klein Gordon equation. The KG equation and SG equation are very similar, and we can find examples of the use of these equations in several physical applications including rigid pendula attached to stretched wires and dislocations which appear in crystals. Moreover, the SG equation offers additional solutions to solitary wave equations which are worth considering in a historical context. The SG equation is given by

$$u_{xt} = \sin(u) \tag{1.8}$$

and the Solution to this equation is given by

$$u(x,t) = 4\arctan\{C\exp(ax + {}^{t}/_{a})\} \tag{1.9}$$

where *C* is an arbitrary integration constant. Equation (1.9) describes a solitary wave solution for the (SG) equation. [1]

The first hint of the usefulness of the *KdV Equation* came in 1955 physicists E. Fermi, J. Pasta, and S. Ulam (FPU) were studying the heat-transfer problem, that is, the flow of incoherent energy in a solid. [1] They modeled this problem in terms of a one-dimensional lattice of equal masses connected by nonlinear springs. FPU attempted to verify via computer simulations to ascertain the dynamical behavior of the chain with non-linear interactions between the atoms. They expected that the initial energy would eventually be shared equally among the degrees of freedom of the simulated lattice. However, much to their surprise, the energy would not share equally among all normal modes, but rather returned in periodic fashion to the originally exited mode and nearby modes. In 1965 the unexpected results of the above simulations motivated physicists N. Zabusky and M. Kruskal to investigate this problem further. [1] The fact that only the long wavelength, lowest-order modes of the lattice contributed to the result led FPU by a continuum approximation to study the *KdV* equation. They discovered via numerical simulations that pulse like waves propagate in a system modeled by the KdV equation. These solitary waves

are able to pass through each other in a collision and preserve their shapes and speed after the collision. The quasiparticle nature of this phenomena led Zabusky and Kruskal to name these waves ***solitons*** from the combination of the words *solitary* in English and the Greek word *on* for *being* later used in physics for the name of *atomic particles*. By using this particle-like nature of solitons and the KdV equation Zabusky and Kruskal where able to form a new model for the continuum approximation of a non-linear atomic lattice with periodic conditions. They found that if they used an initial sinusoidal condition and then launched on the lattice ring, solitons were created and collided with no change in shape or velocity and a very small change to their phase. As time increased these solitons collided at the same point in the lattice and recurrence to the initial state approximately occurred. [3]

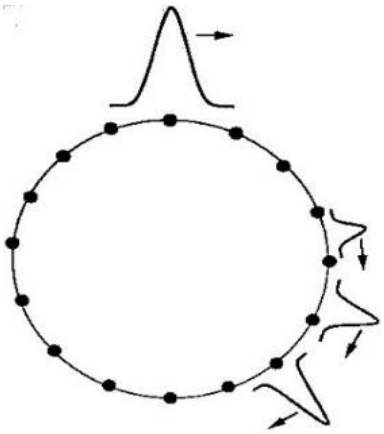

Fig.2 Breaking of an initial state into solitons; the initial state occurs when the solitons collide at the same point. [4]

1.4 Shockwaves

Although we are not studying shockwaves in detail in this thesis, a basic understanding of shockwave dynamics is of primary importance in our investigation of soliton dynamics. It is also of importance to note that both shockwaves and solitons are nonlinear waves and therefore have nonlinear solutions. The above allows us to use some of the numerical and physical models employed in the study of shockwaves in the study of solitons. The formation of both shockwaves and solitons in our experimental result is a product of laser ablation on a metal target, which in the case of the simulation takes the form of a simulated pressure. Furthermore, solitons appear in both simulation and experiment only as a product of the decay of shockwaves. The position of a shockwave can be measured experimentally and in simulations by visual inspection. That is given as certain amount time Δt in nanoseconds has elapsed. The position Δx can be measured in micrometers and later in millimeters. The above is true for both simulation via software and in experiment via shadowgraph photography. The average wave propagation velocity of the shockwave can be obtained as follows. [12]

$$v_{ave}(\Delta t) = \frac{\Delta x}{\Delta t} = \frac{1}{\Delta t}\int_0^{\Delta t} v_S(t')\,dt'$$

where v_S denotes shock front velocity at any given time Δt. Here v_S is used to determine the characteristics of the shockwave. Thus, it is convenient to differentiate the above equation from both sides with respect to Δt in order to obtain the instantaneous velocity as follows

$$v_S(\Delta t) = v_{ave}(\Delta t) + v'_{ave}(\Delta t)\Delta t$$

where the prime denotes differentiation with respect to Δt. The thermodynamic state of the shockwave can be best described by the use of classical *Rankine-Hugoniot* (RH) equations as follows

$$\rho_s(v_s - v_p) = \rho_0 v_s$$

$$Ps + \rho_s(v_s - v_p)^2 = P_0\rho_0 v_s^2$$

$$H_s + \frac{1}{2}(v_S - v_p)^2 = H_0 + \frac{1}{2}v_s^2$$

where ρ_0 is the bulk liquid density, ρ_s is the *helium density* at the front shock. Here, v_s is the shock front velocity, v_p is the *particle velocity* leading to the shock, Ps is the pressure inside the shock, P_0 is the *saturated vapor pressure* of the liquid, H_s is the *helium enthalpy* per unit mass at the shock, and H_0 is the corresponding bulk liquid enthalpy. Values for both ρ_0 and P_0 can be obtained from Ref. [13].

Our last step in this model is to obtain v_p, the *particle velocity* leading to the creation of shockwave front. This can be achieved by the following empirical equation

$$v_p = c_1(v_s - c_0)$$

where c_0 is the speed of sound in the liquid, which in our case is superfluid helium at 1.8 K with a speed of sound of 230 m/s, and $c_1$is a constant that is obtained through calibration against experimental data.

2. Theory of Solitons in ^{4}He

2.1 The Gross-Pitaivski Equation a Non-Linear Schrodinger Equation.

In this section I will discuss the use of the Gross- Pitaivski equation (GPE); a form of the non-linear Schrodinger equation (NLSE) in the context used for the study of superfluidity in ^{4}He. *Superfluidity* in ^{4}He was first observed by Pyotr Kapitsa in 1937 and independently by F. Allen and Donald Meisner and can best be described as a state of matter in which ^{4}He is cooled down to a temperature below 2.17 K at a pressure of 1 atmosphere. The result is a liquid phase with very unusual characteristics. [3] At this phase ^{4}He acquires near zero viscosity, that is, it flows without friction. In the 1950s Landau and Ginzburg modeled superconductivity as a superfluid with the aid the following phenomenological equation [4].

$$i\hbar\frac{\delta u}{\delta t} = -\frac{\hbar^2}{2}\nabla^2 u + gu(|u|^2 - 1)$$

This equation is constructed in the frame of the two-fluid model. Here $|u|^2$ represents the superfluid density, g is a proportional constant with dimensions of energy. However, this equation was found to be difficult to use in the case of Helium. The reason for the above difficulty is because interactions in a liquid such as helium are very strong. Nonetheless, the above Landau-Ginzburg equation up to the first order approximation works very well in the study of the behavior of superfluid helium. The GPE for superfluid Helium is a form of the above equation and is given by

$$i\hbar\frac{\delta\psi}{\delta t} = \left(-\frac{\hbar^2}{2m}\nabla^2 + V_{ext} + g|\Psi|^2\right)\Psi$$

where m is the mass of the Helium atom, $|\Psi|^2$is the atomic density, V_{ext} is an external potential and g is a parameter that measures atomic interactions. It is worth noting here that the GPE has the same mathematical form as the linear Schrodinger equation, plus a non-linear term that takes into account the interaction between the particles. The linear Schrodinger equation is given by

$$i\hbar\frac{\partial\psi}{\partial t} = \left(-\frac{\hbar^2}{2m}\nabla^2 + V_{\text{ext.}}\right)\psi$$

To obtain the GPE equation for use on our system of superfluid ^{4}He we need to first examine the Hamiltonian of such a system.

$$\widehat{H} = \sum_{i=1}^{N}\left(\frac{pi^2}{2m} + V_{ext.}(r_i)\right) + \frac{1}{2}\sum_{i=1}^{N}\sum_{j\neq i}^{N} V\left(|r_i - r_j|\right)$$

where the first term represents the kinetic energy of the i_{th} particle, followed by the external potential acting on it. The final term represents interactions between the N particles in the system.

To find the ground state, we need to minimize the above Hamiltonian. We can achieve this by using the idea from thermodynamic potentials. Using the free energy, we now need to minimize $F = E - \mu N$, where E is the energy and μ is the chemical potential. Thus, from our Hamiltonian we can obtain the variational energy as follows

$$E(\psi) = \frac{\langle \Psi | \widehat{H} | \psi \rangle}{\langle \psi | \psi \rangle}$$

We can now use the above equation to minimize the *free energy F*. Here F is given by

$$F(\psi) = \langle \psi | \widehat{H} | \psi \rangle - \mu \langle \psi | \psi \rangle$$

It is convenient that we proceed by finding the solution in parts. We will calculate each term involved separately. We will begin by finding the kinetic energy term, which is given by

$$\left\langle \psi \left| \sum_{i=1}^{N} \frac{p^2}{2m} \right| \psi \right\rangle = \sum_{i=1}^{N} \frac{\hbar^2}{2n} \int \nabla\psi^*(r_i)\nabla\psi(r_i)\, dr_i$$

$$= N\frac{\hbar^2}{2m}\int |\nabla\psi(r)|^2\, dr$$

$$= -N\frac{\hbar^2}{2m}\int \psi^*(r)\nabla^2\psi(r)\, dr$$

where $\psi(r)$ is the single particle wavefunction. It is important to note that the above equation assumes that our system is comprised of Bosons in their ground state.

We can write potential term as follows

$$\langle\psi|\sum_{i=1}^{N} V_{ext}(r_i)|\psi\rangle = N\int \psi^*_{(r)} V_{ext}\psi(r)\, dr$$

And the interaction term as follows

$$\left\langle \Psi \left| \frac{1}{2}\sum_{i=1}^{N}\sum_{j\neq i}^{N} V(|r_i - r_j|) \right| \Psi \right\rangle$$
$$= \frac{1}{2}\sum_{i=1}^{N}\sum_{j\neq i}^{N}\int dr_i \int \psi^*(r_i)\,\psi^*(r_j) V\left(|r_i - r_j|\right)\psi(r_i)\,\psi(r_j)\, dr_j$$
$$= \frac{N(N-1)}{2}\int dr \int \psi^*(r)\psi^*(r')\, V\,(|r-r'|)\,\psi(r)\psi(r')\, dr'$$

For our last term in the free energy we have

$$\mu\langle\Psi|\Psi\rangle = \mu\left(\int \psi^*(r)\psi(r)\, dr\right)^N$$

To minimize the equations above we need to use calculus of variations. We can begin by working on our equation for interactions as follows

$$\frac{\delta}{\delta\psi^*} < \Psi| \frac{1}{2}\sum_{i=1}^{N}\sum_{j\neq i}^{N} V(|r_i - r_j|)\,|\Psi >$$
$$= N(N-1)\int \delta\psi^*(r)\left(\int |\psi(r')|^2 V(|r-r'|)\, dr'\right)\psi(r)\, dr$$

Followed by the same procedure on our chemical potential term

$$\frac{\delta\langle\Psi|\Psi\rangle}{\delta\psi^*} = N\left(\int \psi^*(r)\psi(r)\, dr\right)^{N-1}\int \delta\psi^*(r)\psi(r)\, dr$$
$$= N\int \delta\psi^*(r)\psi(r)\, dr$$

It is now simple to join all the terms of the free energy and seek for the extremum point:

$$\frac{\delta F}{\delta \psi^*} = N \int \left[-\frac{\hbar^2}{2m} \nabla^2 \psi(r) + V_{ext.}(r)\psi(r) + (N-1)(\int |\psi(r)|^2 V(|r-r'|\, dr')\, \psi(r) - \mu\psi(r) \right] \delta\psi^*(r)\, dr = 0$$

Therefore, the quantity inside brackets vanishes and we arrive at the final form *the time-independent GPE*.

$$-\frac{\hbar^2}{2m} \nabla^2 \psi(r) + V_{ext.}(r)\psi(r) + N\frac{4\pi\hbar^2}{m} a|\psi(r)|^2\psi(r) = \mu\psi(r)$$

where we have used an interaction potential such that $V = (|r-r'|) = \frac{4\pi\hbar^2}{m} a\delta(r-r')$. Here a is the s-wave scattering length and the approximation $N-1 \approx N$ was used to obtain the above equation. This time-independent GPE is a particular case of the time-dependent GPE, therefore we can extend this result to that of the time-dependent case.

2.2 Density Functional Theory for ^{4}He Systems

In our present case we apply density functional theory (DFT) to a collection of ^{4}He atoms at zero temperature. This system can be best described as a Bose-Einstein condensate, that is, all atoms in the system occupy the lowest energy level and the complete system is characterized by a single-particle wave function ϕ_0. [5] The system is characterized by a particle number density given by $\rho = N|\phi_0|^2$ and its kinetic energy in terms of ρ is given by $\tau_s = |\nabla\rho|/4\rho = \left|\nabla\sqrt{\rho}\right|^2$. The ground state configuration of this system is obtained by minimizing the total energy of the system with respect to its single particle wave function. [5,6]

In the case of pure ^{4}He, the density functional is given by

$$E[\rho] = \int \frac{\hbar^2}{2m} \left(\nabla\sqrt{\rho(r)}\right)^2 dr + \frac{1}{2}\int\int dV_{eff}(r-r')\rho(r)\rho(r') + E_c[\rho]\, dr\, dr' \qquad (3.1)$$

By minimizing this functional with respect to $\sqrt{\rho(r)}$ (calculus of variations), the following non-linear Schrodinger equation can be obtained

$$\left\{-\frac{\hbar^2}{2m}\nabla^2 + U_s(\rho, r)\right\}\sqrt{\rho_{(r)}} = \mu\sqrt{\rho(r)} \qquad (3.2)$$

where the non-linear potential is given by

$$U_s(\rho, r) = \int dr' V_{eff}(|r - r'|)\rho(r') + V_c[\rho(r)]$$

Here $V_c = \delta\varepsilon_c \,/\, \delta\rho$, where we take the assumption that ε_c does not depend on the gradients of the density.

It is useful at this point to make use of auxiliary functions defined as follows [6]:

$$U_l^e(r) = \begin{cases} 0, & when\ h < 0 \\ 4\varepsilon\left[\left(\frac{\sigma}{r}\right)^{12} - \left(\frac{\sigma}{r}\right)^{-6}\right], & when\ h \geq 0 \end{cases}$$

$$\tilde{\rho}(r) = \int \rho(r')\Pi_h(|r - r'|)\, d^3r' \ where\ \Pi_h(r) = \begin{cases} \frac{1}{\omega}, when\ r \leq h \\ 0,\ when\ r > h \end{cases} \qquad (3.3)$$

where $\omega = \frac{3}{4\pi h^3}$, the U_l^e function assumes a Lennard-Jones potential at long range and screening at short distance, and the screening distance utilized is h = 2.377Å. furthermore, equation (3.2) provides spherical averaging ($\tilde{\rho}(r)$) for the liquid density.

The effective potential in equation (3.1) includes atom-atom interactions characteristic to Van der Waals systems or asymptotic r^{-6} potentials and screening at short distances. We can remedy this by including a Lennard Jones potential (LJP) in our final functional as well as screening at short distances by a Potential $V_{in}(r)$. LJP and $V_{in}(r)$ are given by

$$V_{eff}(r) = 4\varepsilon\left[\frac{\sigma^{12}}{r} - \frac{\sigma^6}{r}\right], \qquad r \geq h$$

$$V_{eff}(r) = V_{in}(r), \qquad Otherwise$$

For LJP we have several parameters as follows: ε represents the depth of the potential well, σ represents the distance at which the inter-particle potential is zero and r is the distance between the helium atoms. Screening at short distances requires us to make a choice between several forms of the numerical schemes. the above potential takes as a form of the softened potential $V_{in}(r)$. The above choice allows us to take the short-range correlation separately. Many such potentials exist such as OP (Orsay-Paris), BB (Barcelona-Buenos Aires) and OT (Orsay-Trento).

[5,6] We will make use of OT functional. In our case the short-range interaction is treated using the hard sphere approximation.

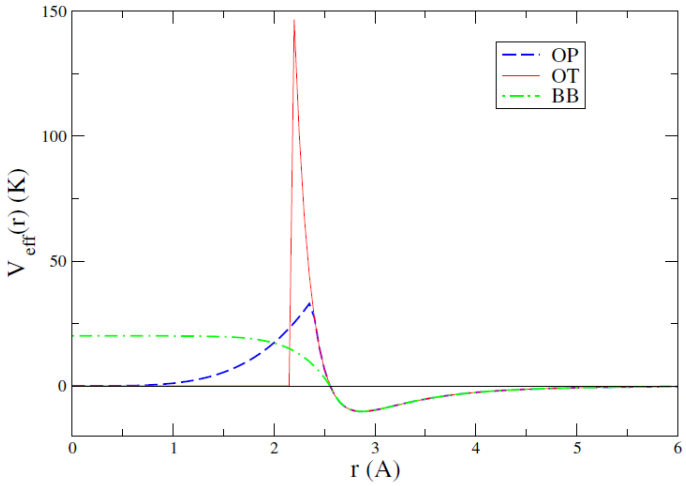

Figure 3 Inner Potentials. [5]

In our final functional we also include the ideas used in the study of classical fluids. Classical fluids can be approximated as a collection of hard spheres or spherical averages. In our case the spherically averaged density is given as follows:

$$\tilde{\rho}(r) = \int dr' \omega(r - r')\rho(r')$$

where we have used a weight function ω (r), given as follows:

$$\omega = \frac{3}{4\pi h'^3}, \qquad r < h$$

$$\omega = 0, \qquad Otherwise$$

The density $\tilde{\rho}(r)$ represents the mean particle density around at point r (i.e., hard sphere with radius h). Furthermore, the value of h needs to match the above potential cut off in LJP. [5,6]

The final form of our OT functional (3.1) is given by:

$$E_{OT} = \frac{\hbar^2}{2m} \int \left|\nabla \sqrt{\rho}\right|^2 d^3r + \frac{1}{2} \iint \rho'(r) U_i^e(|r - r'|)\rho(r')\, d^3r'\, d^3r$$

$$+\frac{c_2}{2}\int \rho(r)\left(\tilde{\rho}(r)\right)^2 d^3r + \frac{c_3}{2}\int \rho_t(r)(\tilde{\rho}(r))^3\, d^3r \qquad (3.4)$$

where the first term in the above equation is the kinetic energy of non-interacting particles, the second term containing U_l^e corresponds to Lennard-Jones potential with parameters σ = 2.556 Å and ε = 10.22 K with complete screening at short distances: $U_l^e = 0 \;\; when\; |r - r'| \leq h,\; h =$ 2.1903 Å. The last two terms correspond to the short-range correlation (hard spheres) with parameters c_2 = 2.411857 x 10^4 K Å^6 and c_3 = 1.858496 x 10^6 K Å^9. [6] Furthermore, by using calculus of variations we can show that the functional obtained for E_{OT} can be minimized in the similar way to equation (3.1) to obtain equation 3.2. The non-linear Schrodinger equation that results from our Orsay-Trento functional (3.3) can be obtain with the following steps.

We can rewrite our above functional as follows:

$$E_{OT}[\Psi] = \frac{\hbar^2}{2m}\int |\nabla\Psi|^2\, d^3r + \frac{1}{2}\iint |\Psi|^2(r)U_l^e(|r-r'|)|\Psi|^2(r')\, d^3r'\, d^3r +$$
$$\frac{c_2}{2}\int |\Psi|^2\left(\tilde{\rho}(r)\right)^2 d^3r + \frac{c_3}{3}\int |\Psi|^2\left(\tilde{\rho}(r)\right)^2 d^3r - \mu\int |\Psi|^2\, dr \qquad (3.5)$$

where we introduced the order parameter Ψ and the lagrangian multiplier μ. Here Ψ is given by $\rho = |\Psi|^2$. We can now take the partial derivative with respect to Ψ as follows:

$$\frac{\delta E_T}{\delta \Psi^*} = -\frac{\hbar^2}{2m}\,\Delta\Psi(r) + \int |\Psi(r')|^2 U_l^e(|r-r'|)\, d^3r'\Psi(r) + \frac{c_2}{2}\left(\tilde{\rho}(r)\right)^2\Psi(r) + c_2\int \Pi_h(|r -$$
$$r'|)\rho(r')\tilde{\rho}(r')\, d^3r'\psi(r) + \frac{c_3}{3}\left(\tilde{\rho}(r)\right)^3\Psi(r) + c_3\int \Pi_h(|r-r'|)\rho(r')\tilde{\rho}(r')^2\, d^3r'\psi(r) -$$
$$\mu\,\Psi(r) = 0 \qquad (3.6)$$

Our final step is to simply rearrange the above equation to obtain the time independent version of the non-linear Schrodinger equation we seek.

$$-\frac{\hbar^2}{2m}\Delta\Psi(r) + V_{eff}(\Psi)\,\Psi(r) = \mu\,\Psi(r) \qquad (3.7)$$

The time dependent version of the non-linear Schrodinger can be obtained in a similar way. We would simply repeat the above process (calculus of variations) on equation (3.4) and include real time in the process.

$$i\hbar\frac{\partial\Psi(r,t)}{\partial t} = \frac{\delta E}{\delta\psi^*} - \mu\Psi(r,t) = -\frac{\hbar^2}{2m}\Delta\Psi(r,t) + V_{eff}(\Psi)\,\Psi(r,t) - \mu\,\Psi(r,t) \quad (3.8)$$

3. Numerical Methods

3.1 Numerical scheme and evaluation of energy.

In this section we describe the static and dynamic properties of superfluid ^{4}He. For this purpose, the Orsay Trento equation (3.8) was solved in three dimensions. We begin by examining equation (3.8) which in this case is being considered in position representation. We can use the (FFT) Fast Fourier transform method to evaluate our kinetic energy and & *nonlinear potential* $V_{eff.}$ in the above equation. A 3D Cartesian grid is used for spatial discretization of our order parameter. For the time integration of equation (3.8) and the evaluation of its kinetic and Potential energy terms we applied an *operator splitting scheme*. [9] The OT functional equations (3.5) and (3.6) contain integrals in the nonlinear potential that appear as convolutions or more specifically between the liquid density and the screened Lennard-Jones potential. Since equation (3.8) is subject to boundary conditions we can simplify this calculation by realizing that the convolution reduces to a local multiplication operation in Fourier space. In our case to calculate the above integrals we use two forward FFTs and one backward FFT. We have also used the above method on the spherical average terms present in equations (3.5) and (3.6). [6] To evaluate our FFT we have used the (FFTW) Fastest Fourier Transform in the West package, for which a parallel implementation using threads or shared memory computer is available. FFTW uses many FFT algorithms and a planner within FFTW methods to choose the best set of algorithms to use for each calculation. This is accomplished by measuring the speed of different combinations of algorithms. In our case, the FFT step determines the overall computational cost of the method. The above energy and time propagation schemes have a computational cost of $O(N^3 \log N)$ operations. where N is the total number of grid points along each axis.

3.2 Time-space discretization of DFT equation

For the time-space discretization of our DFT equations we can start by considering equation (3.8), which is a time-dependent nonlinear Schrodinger equation of the form:

$$i\hbar \frac{\partial \Psi(r,t)}{\partial t} = \widehat{H}\psi(r,t) \qquad (3.9)$$

where H is a DFT operator consisting of kinetic ($\hat{T}$) and potential ($\hat{V}$) contributions, $\widehat{H} = \hat{T} + \hat{V}$. The solution to the above equation is given by

$$\Psi(r, t+\Delta t) \approx \exp\{-(i/\hbar)\int_{t}^{t+\Delta t} \widehat{H}\Psi(r,t')\,dt'\}\,\psi(r,t) \approx \exp\{-(i/\hbar)\widehat{H}[\Psi(r,t)]\Delta t\}\psi(r,t)$$

here the total energy operator is *splitted* into its components and given as follows:

$$\hat{T}: e^{-i\hat{T}t/\hbar}\Psi(t)$$

$$\hat{V}: e^{-i\hat{V}t/\hbar}\Psi(t)$$

The propagation of the *splitted* operators $\hat{T}$ and $\hat{V}$ over time Δt is done by the following scheme: We first propagate $\Delta t/2$ for $\hat{\tilde{T}}$, followed by the propagation Δt for $\hat{\tilde{V}}$ and as our final step we propagate $\Delta t/2$ for $\hat{\tilde{T}}$. Thus, in total we propagate Δt for both $\hat{T}$ and $\hat{V}$. [8] In the case of our potential term $\hat{V}$, it is simple to see that the calculation is straight forward, since the potential $\hat{V}$ is a simple number. Thus, the propagation is simply a multiplication:

$$\Psi(t+\Delta t) = e^{-i\hat{V}\Delta t/\hbar}\Psi(t)$$

For the propagation of *kinetic energy*, we have a true *operator* $\hat{T}$.

$$\Psi(t+\Delta t) = e^{-i\hat{T}\Delta t/\hbar}\Psi(t)$$

Thus, we need to first apply forward FFT, evaluate the second derivative (Laplacian) in the Fourier space, and then execute backward FFT. The second derivative in the Fourier space corresponds to multiplication by the wave vector squared. [8]

To better account for the non-linear potential, the following *predictor-corrector* algorithm is used. The first step of this method is to calculate an estimate for the desired wavefunction we wish to propagate in our simulation. [9,10]

$$\psi_{Pred.}(t+\Delta t) = e^{-it\hat{V}[\psi(t)]/\hbar} \cdot \psi(t)$$

We can now follow by constructing a corrector step. This new step takes the above prediction and corrects it by refining our initial approximation.

$$\hat{V}_{Corr.} = \frac{\hat{V}[\psi_p]+\hat{V}[\psi(t)]}{2}$$

We then proceed to propagate the new corrected result as follows:

$$\hat{V}_{Corr.}: \Psi_{Corr.}(\psi + \Delta t) = e^{-it\hat{V}_{Coor.}/\hbar} \cdot \psi(t)$$

Thus, the potential that is used for the actual propagation is an average of the present and future potentials.

4. Experimental observations of solitons in Helium superfluid

4.1 Solitons in ultracold materials

To date solitons have been studied in a variety of media. In the case of ultracold materials, solitons have been investigated in Bose Einstein Condensates (BEC) at near absolute zero temperature by several theoretical methods. These methods use make use of the Gross-Pitaevskii equation with time-dependent parameters to model the above phenomena [15,16]. Experimental methods have also been employed. In particular the dynamics of BEC in an optical lattice have been studied by the harmonic trap method. Motion is created in these methods by displacing the harmonic trap. Moreover, as the condensate undergoes critical displacement the BEC undergoes Bragg reflection. The first of this Bragg reflections generates a train of solitons and destabilizes the BEC triggering explosive expansion. [14,15] In the case of helium superfluid, solitons have also been studied in detail for decades. However, the clear majority of both theoretical and experimental research has been focused on superfluid ^{3}He, while superfluid ^{4}He has only been studied in until more recent times. Among the first these investigations into superfluid ^{3}He is the study of moving domain walls or plane solitons modeled by Ginzburg-Landau equations (GLE). In this case solitons where created magnetically and where found to relax into a composite soliton.[17] Solitons have also been observed to include both planar and linear solutions. This can be found by applying the method of the conventional homotopic groups and GLE equations to magnetically created waves in of ^{3}He superfluid. [18] In related research, linear solitons have also been observed to be particle like in specific cases. In the study of particle like solitons both phases A and B of superfluid ^{3}He where considered. Solitons in phase B where found to be unstable. However, phase A solitons possess a type of momentum that stabilizes the soliton size and allows the soliton to reach equilibrium shape and velocity. Asymptotic solutions of GLE where used to describe the dynamics of the above waves. [19]

More recently research into solitons in superfluid He has focused primarily on ^{4}He thin films absorbed on supporting substrates. The study of ^{4}He thin films goes back several decades and has not been thoroughly investigated. However, the above research offers the greatest similarity to the study of solitons in bulk superfluid ^{4}He. Experiments on monolayer superfluid helium films indicate that nonlinear third sound excitations and small amplitude effects can be created by localized perturbations in the superfluid density. The above perturbations where observed to evolve into ordered string of solitons and shockwaves. It is important to note here that no dissipation was observed in these experiments for solitons. Rather, solitons propagate undistorted. Furthermore, it is expected that at sufficiently low temperatures superfluid solitons would become the dominant modes of excitation. [20] The thickness of the thin films in these experiments typically have dimensions of the order of 10^{-7}cm and solitons are created via heat pulses on the superfluid film, resulting in a train of solitons. This method of producing solitons has been in the past modeled with both KdV and GP equations. [7, 21] In the case *superfluid ^{4}He in bulk liquid solitons* had *not* previously been observed. One reason for the above is a lack of theoretical models of bulk superfluid helium until recently. Both KdV and GP equations cannot be applied to bulk superfluid ^{4}He due to a lack of accuracy in atomic scale dynamics of these models. However, we can apply models such as DFT to bulk superfluid ^{4}He, since DFT can describe atomic scale dynamics and static response accurately.

4.2 Experimental Observations of solitons in bulk ^{4}He superfluid

The main difference between the above thin films experiments and our experiment is that our experiment is carried out in ^{4}He bulk liquid, while thin film experiments are carried in the presence of a film supporting substrate and are therefore two-dimensional in nature. The ^{4}He bulk liquid experiment is a three-dimensional system. In the latter experiment a focused laser pulse is used to generate plasma on the surface of a solid copper target that is immersed in bulk superfluid helium. [11]

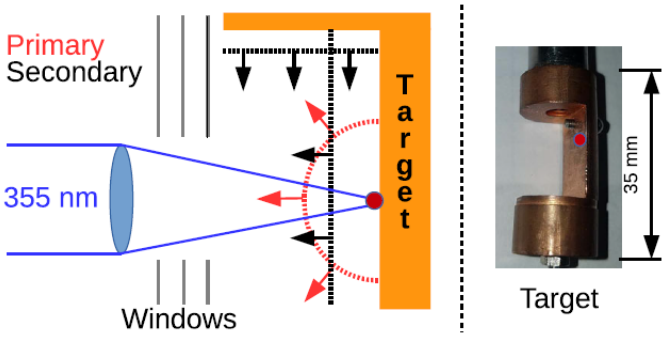

Figure 4 Solid metal target immersed in bulk superfluid helium. [11]

The initial expanding plasma leads to nonlinear excitation of the surrounding liquid, which is visualized by a time-resolved shadowgraph photography technique. Here a delayed laser pulse is used as the background light.

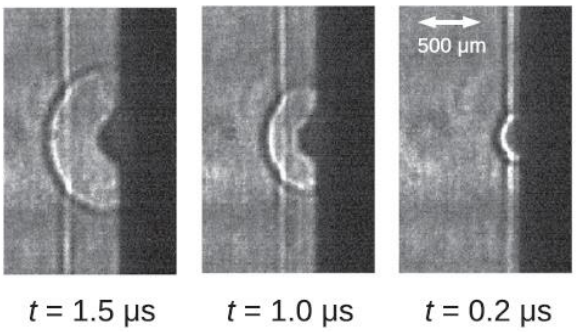

Figure 5 Shadowgraph snapshots of the waves emitted from the target at given times *t*.

In *Figure 5* we can observe how expanding plasma produces a primary spherical geometry wave emission. We can also observe a secondary planar wave emission is produced by boiling of liquid helium on the target surface and the subsequent rapid gas expansion. In the long-time regime (t > 19 μs) they were at first tentatively assigned as solitons since both waves propagate in superfluid helium without dispersion.

5. Discussion

5.1 Numerical Result

In this section I present the results of three TDDFT simulations. The above simulations where coded in the C programming language and make use of DFT, the Orsay-Trento equation (3.8), FFT methods, time-space discretion of DFT and other computational methods described in our numerical methods section. The simulations return data every one thousand steps up to hundreds of thousands of steps. Each of these steps contains a 'snapshot' of the current state of the simulation. Both shockwave and soliton propagation were observed in the results of these simulations. Distance traveled by the shockwaves and solitons is measured in nanometers, while time is measured in pico-seconds. The data obtained from the simulations was then analyzed using *grace*. In Figure 6 you can see a snapshot of one of these simulations.

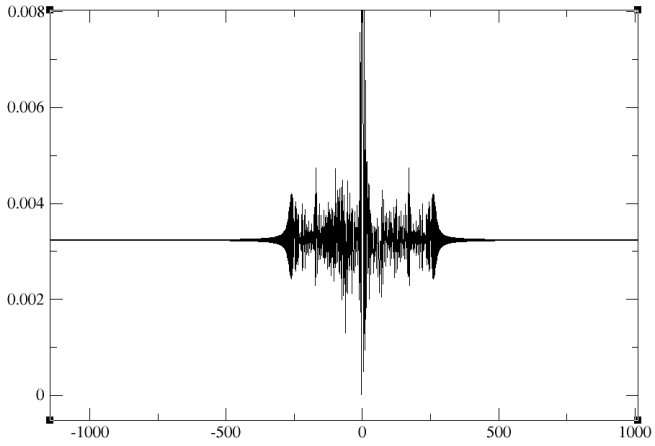

Figure 6 Soliton and Shockwave propagation result.

(y-axis: Density in Bohr^3, x-axis: Distance in Bohr).

Solitons where observed in our simulations under certain conditions. Mainly, solitons appear to inhabit a domain characterized by a propagation velocity above the speed of sound in ^{4}He superfluid (280 m/s) to approximately 665 m/s. Solitons above this domain where found to be unstable and below the above domain no solitons where observed. In this section I will also show how the results of all simulations help support the existence of solitons in bulk ^{4}He superfluid. Although initially unclear from the experimental results, the behavior of the observed secondary waves hinted at the presence of solitons. This led us to create a series of simulations to further explore the problem. The simulation results contain not only the shockwaves which were observed in the experimental result, but also elements of secondary shockwaves and soundwaves. It is among these other non-shockwave components of the simulation that we find solitons. Furthermore, the soliton waves observed do not dissipate over time, rather they appear to reach an equilibrium amplitude, width, and velocity.

Solitons in our simulation can be better understood in the context of shockwave formation and propagation. In general, we can say that shockwaves are produced as an effect of the initial induced pressure, which in our case takes the place of laser ablation and rapid expansion of plasma in our experimental section. However, the resulting compression and rapid expansion of bulk ^{4}He superfluid produces not only shockwaves but also solitons. It is clear from both simulations and experimental results that the shockwaves produced are then followed by slower decaying waves which turn into solitons. It is important to note that the temporal and spatial scales used in the experimental section are in the order of *microseconds* and *micrometers*. While the simulations were performed in *nanometers* and *picoseconds* scales. However, it is clear that we can rescale either the simulation or the experimental section to match either scale.

5.2 Shockwave Velocities

Shockwave velocity behaved predictably throughout the simulations carried out. In figure 7 it is shown that for our first TDDFT simulation a shockwave was formed at 1.51 pico-seconds and had an initial propagation velocity just above 942 m/s. The shockwave then undergoes exponential decay until the end of the simulation. The shockwave was formed by using the following parameters in our simulation: We used a gaussian function with amplitude equal to approximately 5.5 times the bulk density of ^{4}He superfluid liquid (0.021836 Å^{-3}) and a width of 2 Bohr or approximately 1Å.

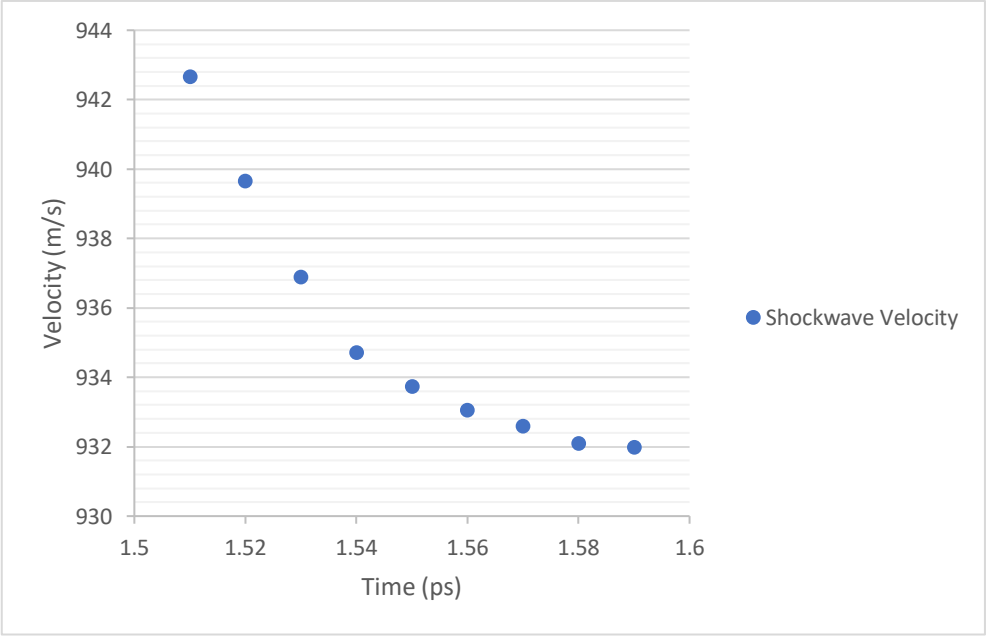

Figure 7 Shockwave velocity for simulation 1

Gaussian wave with amplitude: 5.5 times bulk density (0.021836 Å^{-3}) and Width: 2 Bohr.

By increasing the initial density to 8.5 times the bulk density of ^{4}He superfluid liquid while keeping the initial width of the gaussian function at 2 Bohr, the velocity of the following shocks was observed to increase. For the second simulation shown in figure 8 a shockwave was formed at 1.50 pico-seconds and had a propagation velocity of approximately 1063 m/s. The shockwave for our second simulation also then undergoes exponential decay until the end of the simulation.

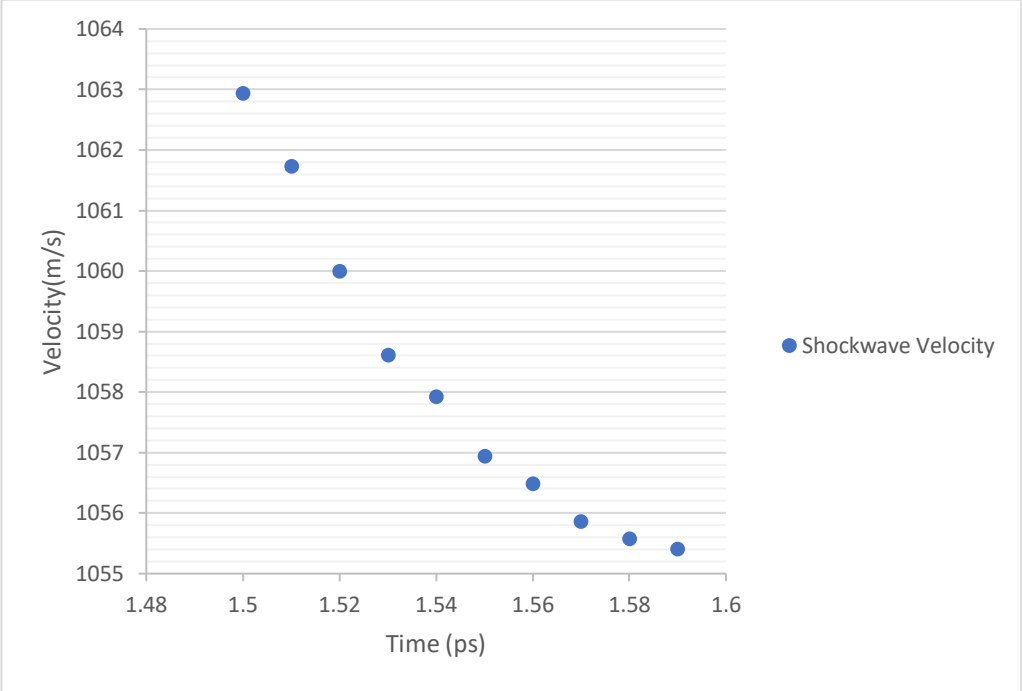

Figure 8 Shockwave velocity for simulation 2.

Gaussian wave with amplitude: 8.5 times bulk density (0.021836 $Å^{-3}$) and Width: 2 Bohr.

For our third and final simulation shown in Figure 9, the initial density was increased to 11.5 times the bulk density of ^{4}He superfluid liquid while keeping the initial width of the gaussian function at 2 Bohr. A shockwave was formed at 0.85 pico-seconds and had a propagation velocity of approximately 1257 m/s. The shockwave then also undergoes exponential decay until the end of the simulation. Solitons were observed in all three simulations presented above. The soliton component of all three simulations will be covered in the next section.

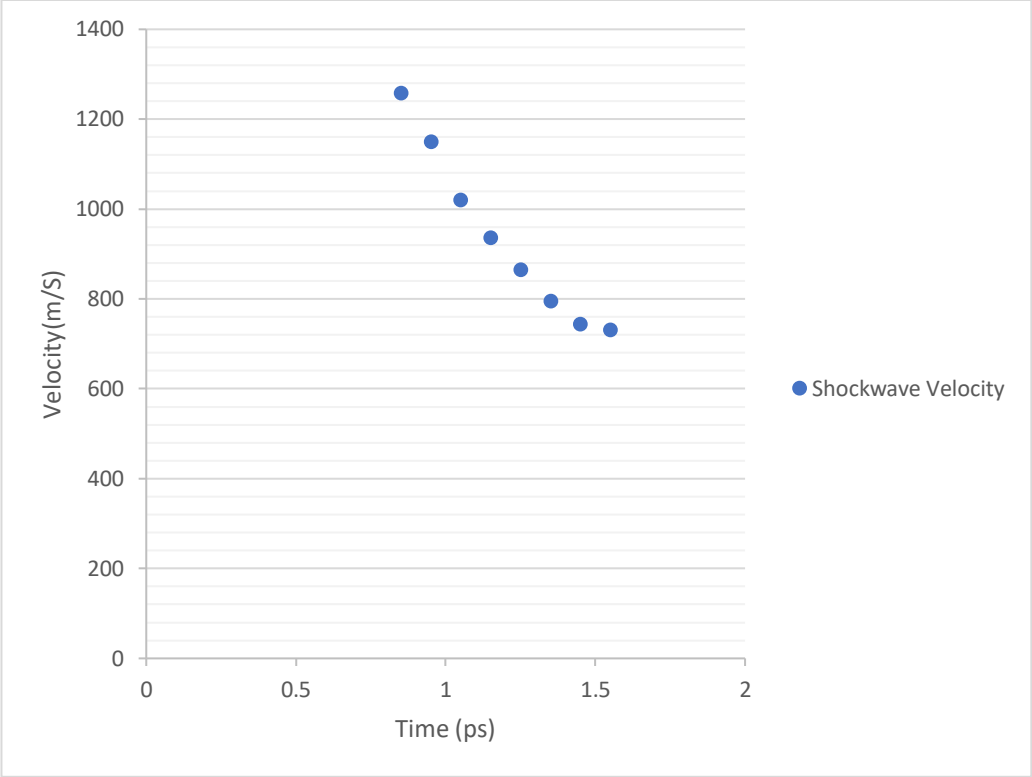

Figure 9 Shockwave velocity for simulation 3.

Gaussian wave with amplitude: 11.5 times bulk density (0.021836 $Å^{-3}$) and Width: 2 Bohr.

5.3 Soliton Velocities

Increasing the initial pressure in the above simulations is a good way to gain a better understanding of the behavior of the system. In particular, solitons become unstable past a certain velocity in bulk ^{4}He superfluid. In figure 10 we can see the dynamics of formation of the soliton wave observed for our first simulation. After initial compression and following the formation of shockwaves, the sound wave in our first simulation can be seen decreasing in velocity. As time progresses a soliton wave is created as a product of the decay of the shockwaves present in the system. A soliton was formed for our first simulation at 1.35 ps and can be seen maintaining equilibrium velocity to the end of the simulation. In contrast to shockwaves, soliton waves were observed to travel at an equilibrium velocity of approximately 428 m/s. This velocity is the slowest velocity we investigated for a soliton traveling in bulk ^{4}He superfluid and appears a good starting point above the speed of sound in He^4 superfluid (230 m/s). No solitons where observed below the equilibrium velocity of our first simulation.

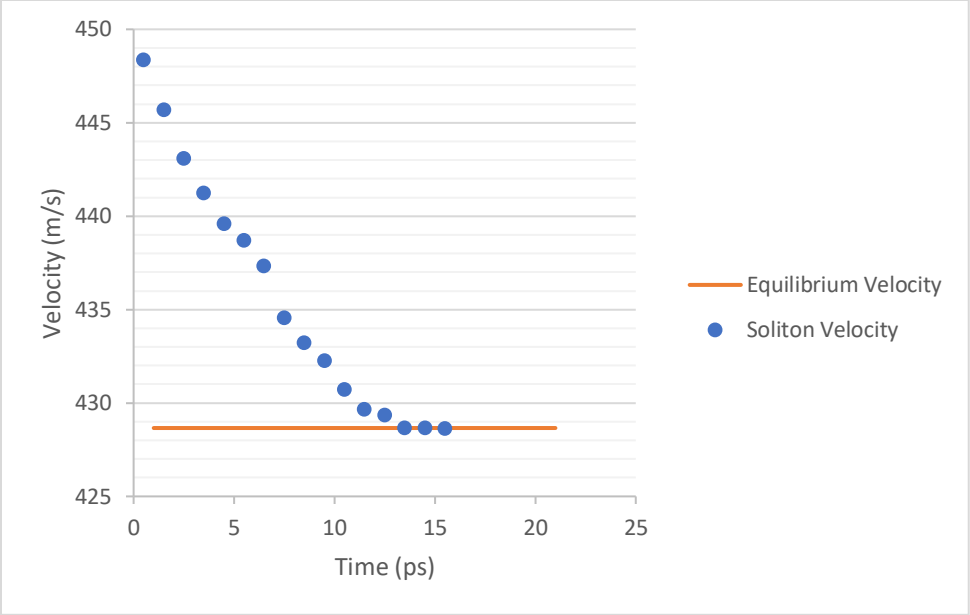

Figure 10 Soliton velocity for simulation 1.

Gaussian wave with amplitude: 5.5 times bulk density (0.021836 $Å^{-3}$) and Width: 2 Bohr.

For our second simulation shown in figure 11. A soliton wave is formed at 1.35 ps and can be seen traveling at an equilibrium velocity of 505 m/s. The soliton maintains the above equilibrium velocity to the end of the simulation. As in the case of our first simulation, it is of interest here that the soliton reached equilibrium velocity and maintained that velocity until the end of the simulation. Once again showing this crucial detail unique to solitons.

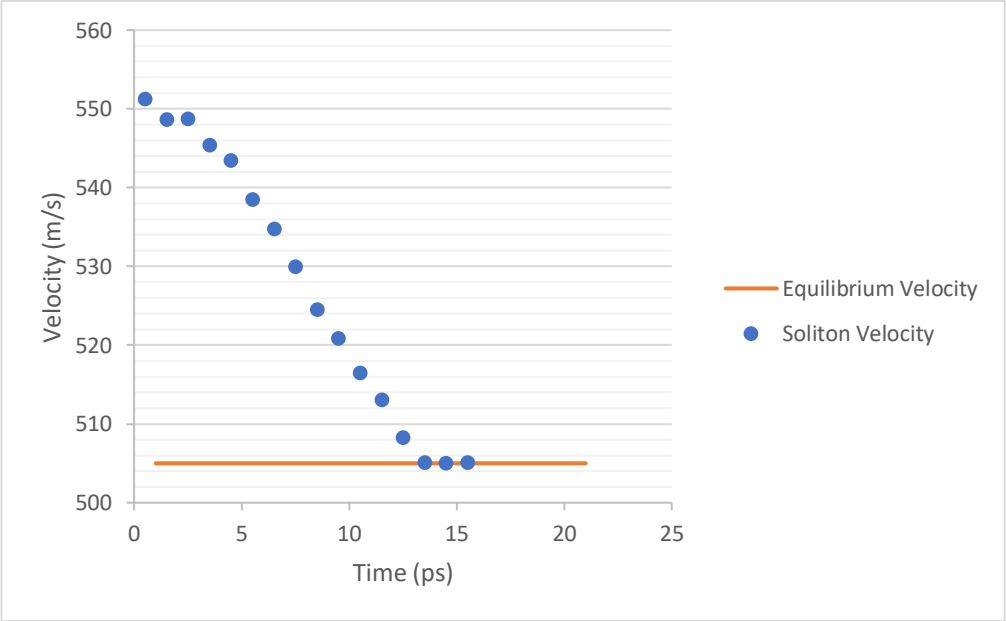

Figure 11 Soliton velocity for simulation 2.

Gaussian wave with amplitude: 8.5 times bulk density (0.021836 $Å^{-3}$) and Width: 2 Bohr.

For simulation 3 a soliton wave was formed at 1.35 ps as can be seen in Figure 12. Equilibrium velocity for this soliton was achieved at a velocity of 661.5 m/s. Here too, the soliton wave traveled at equilibrium velocity until the end of simulation.

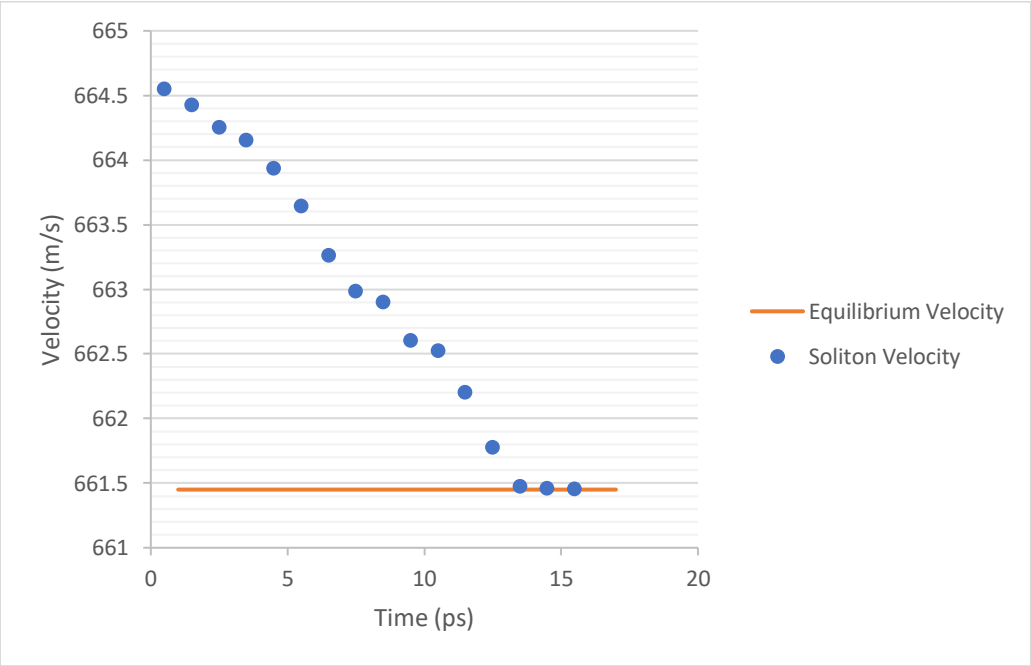

Figure 12 Soliton velocity for simulation 3.

Gaussian wave with amplitude: 11.5 times bulk density (0.021836 $Å^{-3}$) and Width: 2 Bohr.

It is important to note that simulation three represents the *end* of the possible *stable velocity* for soliton wave activity observed in bulk ^{4}He superfluid. Soliton waves traveling faster than these speeds where found to be *unstable* and usually disappeared from the simulation during or immediately after formation and cannot be considered true solitons.

5.4 Soliton Halfwidth

Soliton waves exhibit no change in width as they travel. In order to ascertain that the waves produced are indeed solitons, the half width of the above waves was measured throughout all simulations. The measurements and figures 13-15 indicate that no dispersion occurs for the soliton waves in all our simulations. For simulation 1 we observed a halfwidth of 8.0 Å.

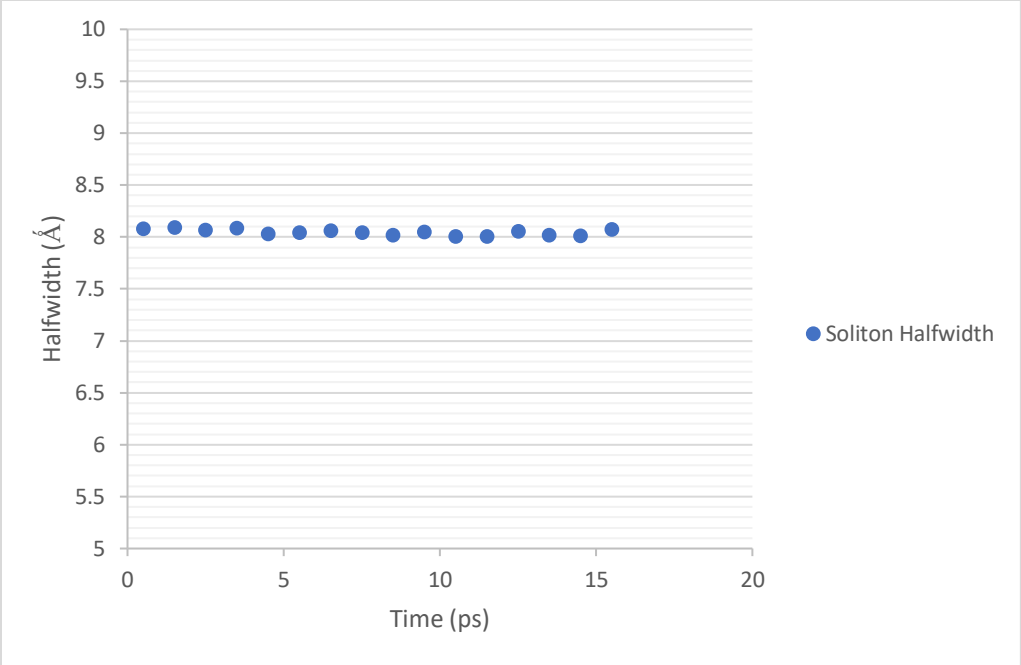

Figure 13 Halfwidth for Soliton in simulation 1.

Gaussian wave with amplitude: 5.5 times bulk density (0.021836 $Å^{-3}$) and Width: 2 Bohr.

For simulations 2 and 3, a similar trend was observed. That is, the width of the soliton remained static throughout the simulation. This can be seen in figures 14 and 15.

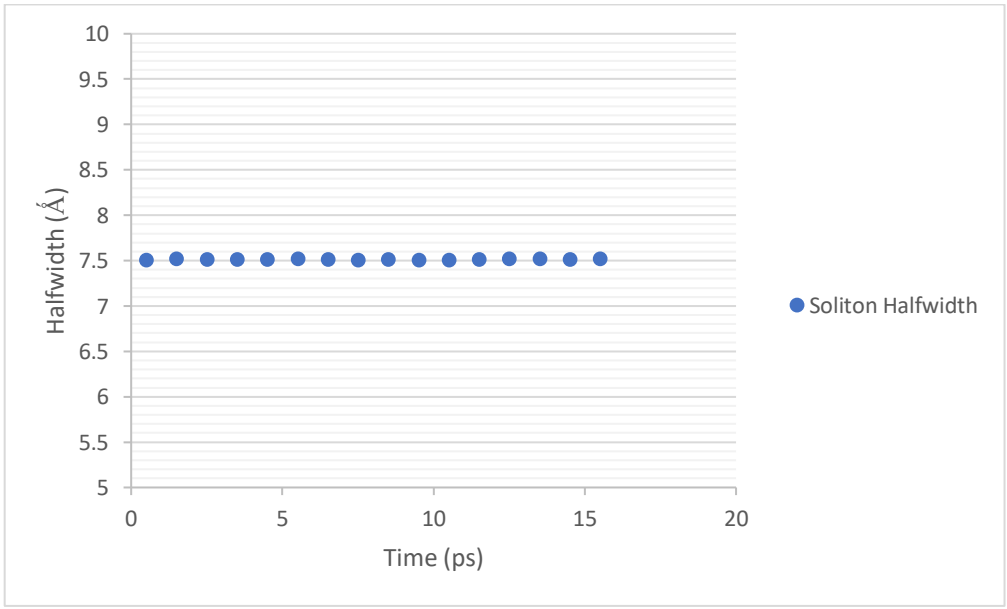

Figure 14 Halfwidth of Soliton for simulation 2.

Gaussian wave with amplitude: 8.5 times bulk density (0.021836 $Å^{-3}$) and Width: 2 Bohr.

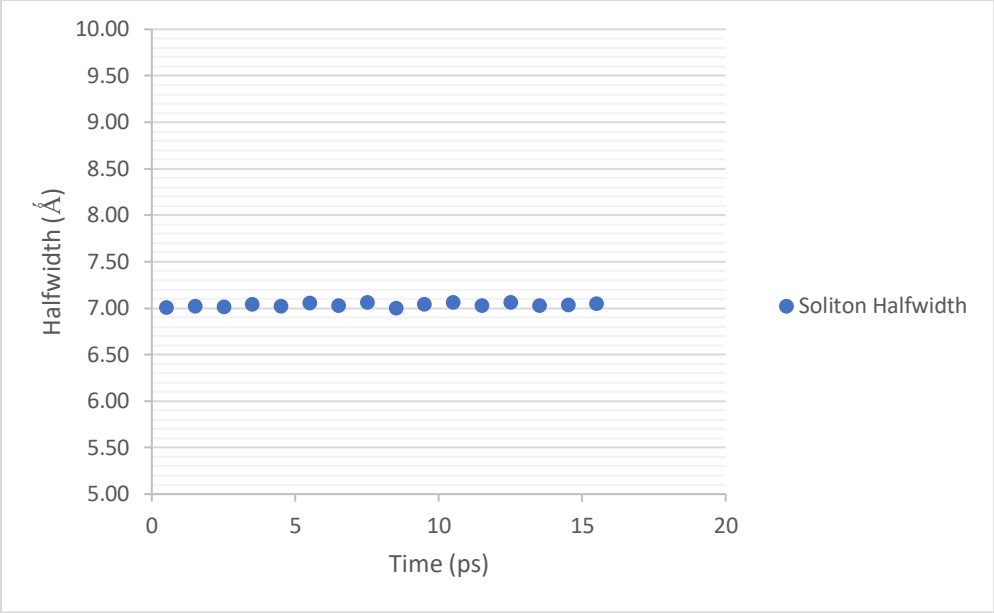

Figure 15 Halfwidth of Soliton for simulation 3.

Gaussian wave with amplitude:11.5 times bulk density (0.021836 Å^{-3}) and Width: 2 Bohr.

For simulation 2 we observed a halfwidth of 7.5 Å and for simulation 3 the halfwidth obtained is approximately 7.0 Å. It is of importance to note here that for figures 13-15 measurements were carried out by visual inspection. Any variation in the half-width of each of these figures is due to the limitations of the measuring method used. This data provides further positive proof that the waves observed are indeed solitons. Moreover, a clear relationship can be seen between the force applied to create the initial waves and their width. That is, higher initial density produces solitons with higher propagation velocity and smaller half-width.

5.5 Density

The relationship between density and velocity was also studied. For shockwaves it can be seen in figure 16 that as density increases in simulations 1 through 3, so does the propagation velocity of the shockwaves produced.

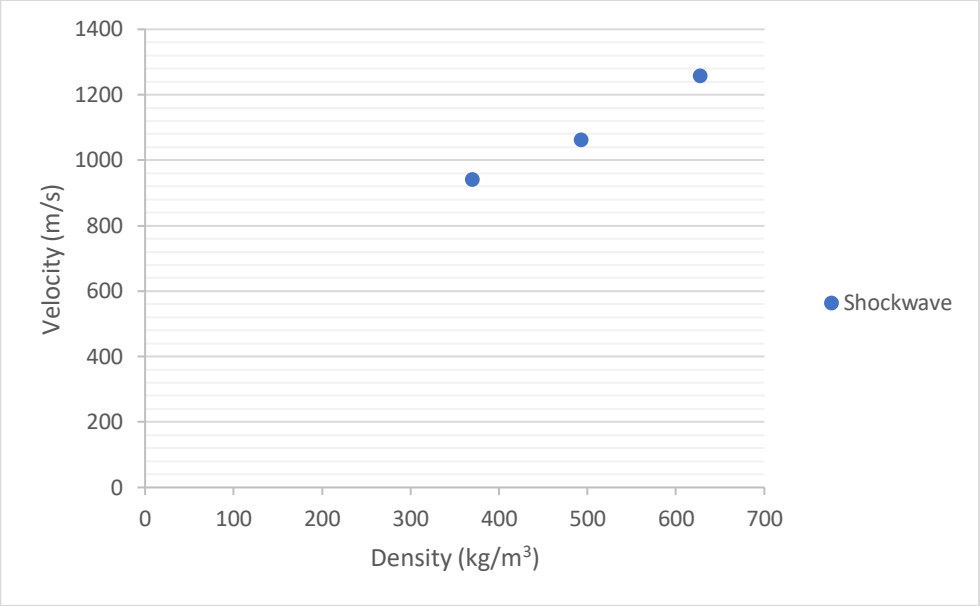

Figure 16 Density-velocity for shockwaves. Gaussian wave with amplitude: 5.5, 8.5 and 11.5 times bulk density (0.021836 $Å^{-3}$). Width: 2 Bohr. Each point comes from an independent simulation.

In the case of the solitons the equilibrium velocity of each simulation increases as shown in figure 17. The velocities in figure 17 were taken from the equilibrium velocities of solitons in simulation 1 through 3.

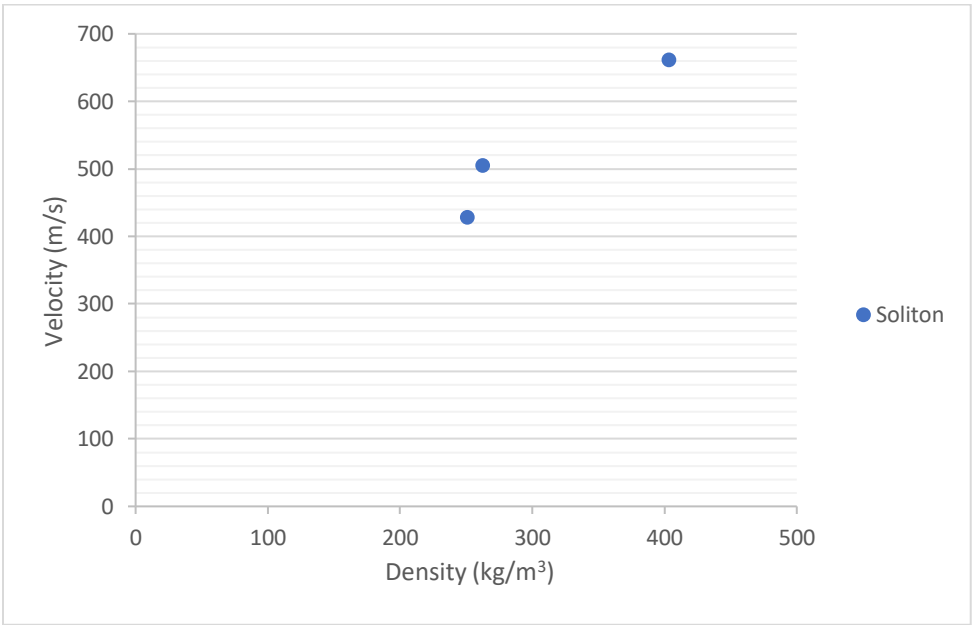

Figure 17 Density-velocity for solitons. Gaussian wave with amplitude: 5.5, 8.5 and 11.5 times bulk density (0.021836 $Å^{-3}$). Width: 2 Bohr. Each point comes from an independent simulation.

It is important to note here that the density measured for shockwaves, shown in figures 16 is higher throughout all simulations when compared to the density measured for solitons, shown in figure 17. This is to be expected since unlike shockwaves, which are already present in the initial stages of our simulations, solitons appear much later in the simulations and can only be observed after shockwaves are gone from the simulation. The observed trend is therefore in agreement with theoretical models, in general, denser liquids yield faster velocities.

5.6 Soliton Amplitude

The amplitude of the soliton waves produced was also analyzed for all simulations. Amplitude remained constant for all solitons throughout individual simulations. The velocity of the solitons increased as both their respective initial pressure and consequently their amplitudes increased. Amplitude and velocity profiles for simulations 1 through 3 are shown in figure 18.

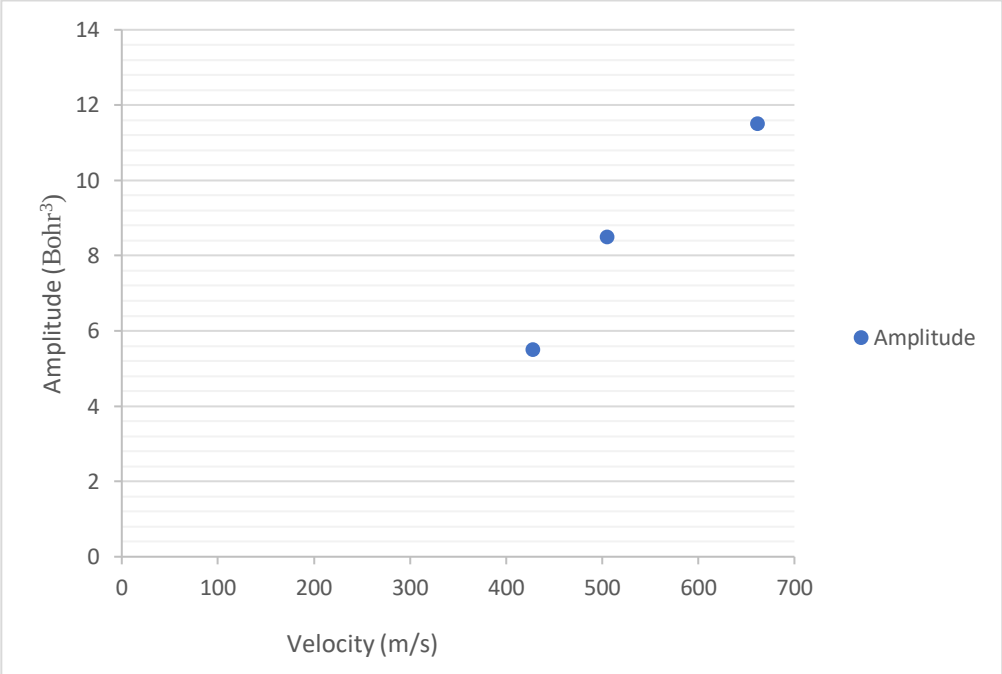

Figure 18 Soliton Amplitude-Velocity. Amplitude is in units of bulk density: Bohr^3 Gaussian wave with amplitude: 5.5, 8.5 and 11.5 times bulk density (0.021836 Å^{-3}). Width: 2 Bohr. Each point comes from an independent simulation.

Soliton waves exhibit no change in amplitude as they travel. In our simulation results we observed no change in amplitude for all soliton waves produced. Furthermore, in our simulations the soliton waves observed can be seen travel at a higher speed for higher amplitudes (figure 18).

5.7 Soliton Final Result

The results of our simulations prove that the waves observed in the experiential result are solitons. Furthermore, the solitons observed propagate undistorted and are free from the effects of dissipation. In our publication we presented the following graph [11]:

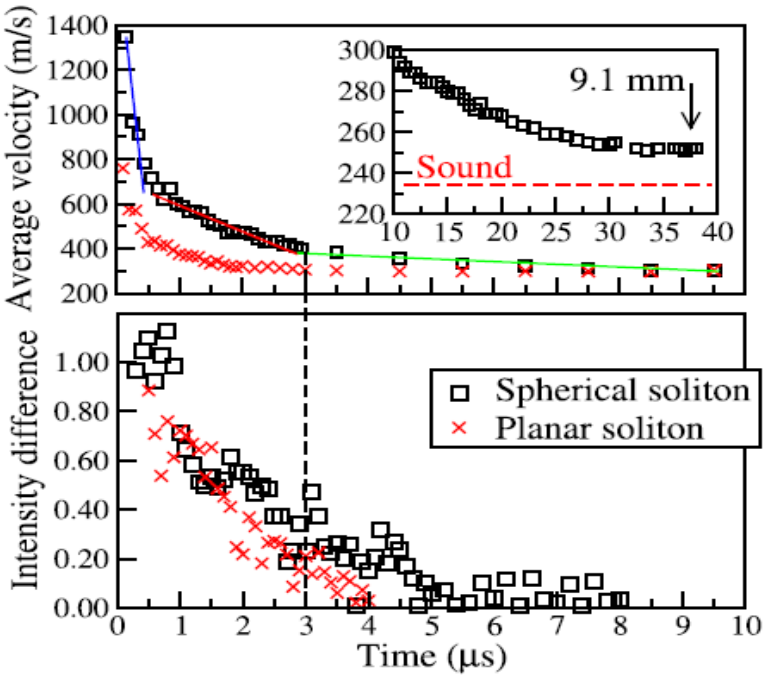

Fig. 19. Time evolution of the averge soliton velocity at 1.7 K. The three lines (blue, red, green) highlight the changes in the wave deceleration. The time axis refers to the delay between the ablation and backlight laser pulses. The bottom panel shows the normalized shadowgraph intensity difference in front of the wave vs behind it. [11]

Figure 20 shows that solitons in ^{4}He superfluid propagate at velocities between 280 m/s to approximately 435 m/s. In the simulations I have presented in this thesis, solitons propagate faster. Although the above graph indicates the domain for soliton propagation is comprised of slower velocities, the region from 435 m/s to under 680 m/s was not investigated at the time of its publication. The possibility that the soliton region for propagation velocity in this graph extends up to approximately 680 m/s, is not problematic to either result. The region in the graph this affects is the red line between the green and blue lines on the top panel. This new result fits in well with the overall picture of soliton propagation velocities obtained throughout all simulations carried out for both the above publication and this thesis. No solitons where observed past 680 m/s. All solitons for velocities above 680 m/s were found to be unstable and would simply distort and disappear from the simulation. Furthermore, in the above graph the blue line represents the domain for the velocities of shockwaves. Since, we have discovered through our simulations that solitons are a product of shockwave decay, it is *not* unreasonable for soliton velocities to extend from this region, down towards the speed of sound in ^{4}He superfluid.

6. Conclusion

6.1 Solitons in bulk ^{4}He superfluid

In this thesis we have investigated the presence of solitons in bulk ^{4}He superfluid. Solitons can be best described as self-reinforcing non-dissipative solitary waves that maintain their speed and shape upon collision with other such waves. We have employed simulations to ascertain if the waves observed in our experiments are indeed solitons. The result of our simulations prove that soliton waves are indeed present in in bulk ^{4}He superfluid. Solitons in ^{4}He superfluid, are still a new area of study and very likely to offer new science. For future work it may be possible to study the dynamics of soliton distortion and break apart dynamics at shockwave velocities. As stated above these solitons break apart after formation. The complete picture or specific reasons for their distortion and disappearance form the simulations has not yet been completely determined.

References

1. P.G. Drazin, R.S. Johnson, *Solitons: An Introduction*, Cambridge University Press, 1989.

2. Russel John Scott Report on the fourteenth meeting British association for the advancement of science: *Report on waves*, London John Murray, 1845.

3. Michel Remoissenet, *Waves called Solitons*: *Concepts and Experiments 3rd revised ed.*, Springer,1995.

4. Rogel-Salazar, J. "*The Gross–Pitaevskii Equation and Bose–Einstein Condensates*." European Journal of Physics, vol. 34, no. 2, Sept. 2013, pp. 247–257.

5. Francesco Ancilotto et al. "*Density Functional Theory of doped superfluid liquid helium and nanodroplets."* Int. Rev. Phys. Chem. 36, 2007, pp. 621.

6. Lehtovaara, L., et al. "*Efficient Numerical Method for Simulating Static and Dynamic Properties of Superfluid Helium*." Journal of Computational Physics, vol. 194, no. 1, 2004, pp. 78–91.

7. S. Nakajima, S. Kurihara, and K. Tohdoh, "*Solitary waves in saturated films of superfluid 4He*." J. Low Temp. December 1980, Volume 41, Issue 5–6, pp 521–528.

8. Steven G. Johnson, "*Notes on FFT-based differentiation, MIT Applied Mathematics*". NotesonFFT-Baseddifferentiation - MIT Mathematics, 1980, Phys. 39, 465.

9. Press, William H., et al. *Numerical Recipes in C: The Art of Scientific Computing/Press,* W.H Cambridge University Press, 1992.

10. Scheid, Francis. *Numerical Analysis*. McGraw-Hill, 1968.

11. Ancilotto, Francesco, et al, "*First Observation of Bright Solitons in Bulk Superfluid He4*." Physical Review Letters, 2018, vol. 120, no. 3.

12. Eloranta, Jussi, et al. *"Time-Resolved Study of Laser Initiated Shock Wave Propagation in Superfluid 4He."* The Journal of Chemical Physics, 2016, vol. 145, no. 12, 124504.

13. R. J. Donnelly and C. F. Barenghi, *"The observed properties of liquid Helium at saturated vapor pressure."* J. Phys. Chem., 1998, Ref. Data 27, 1217.

14. Scott, R. G., T. M. Martin, A. M. Fromhold, F. W. Bujkiewicz, S. Sheard, and M. Leadbeater, *"Creation of Solitons and Vortices by Bragg Reflection of Bose-Einstein Condensates in an Optical Lattice."* Phys. Rev. Lett., 2003, 90, 110404.

15. Z. X. Liang et al., *"Sound speed of a Bose-Einstein condensate in an optical lattice."* Phys. Rev. Lett., 2005, 94, 050402; B. Li et al., Phys. Rev. A 2008, 78, 023608.

16. Rajendran S, Muruganandam P and Lakshmanan, *"Bright and dark solitons in a quasi 1D Bose-Einstein condensates modelled by 1D Gross-Pitaevskii equation with time-dependent parameter."* M Physica D, 2010, p. 239-366.

17. 'K. Maki and P. Kumar, *"Composite Magnetic Solitons in Superfluid ^{3}He-A".* Phys. Rev. Lett. 38,1977, p. 557.

18. V. P. Mineyev and G. E. Volovik, *"Planar and linear solitons in superfluid ^{3}He."*, Phys. Rev. B, 1978, 18, 3197.

19. G. E. Volovik and V. P. Mineev, Zh. Zh. Eksp., "Particle like solitons in superfluid *^{3}He phases."* Teor. Fiz. August 1977, 73, pp. 767-773 [Sov. Phys. -JETP].

20. B. A. Huberman, *"Superfluid solitons in Helium films."*, Phys. Rev. Lett., 1978, 41, 1389.

21. C.A. Condat and R.A. Guyer. *"Soliton resonances in Helium films."* Phys. Rev., 1982, 825, 3117.

Appendix
Publication on Physical Review Letters.

PHYSICAL REVIEW LETTERS 120, 035302 (2018)

First Observation of Bright Solitons in Bulk Superfluid ^{4}He

Francesco Ancilotto,[1] David Levy,[2] Jessica Pimentel,[3] and Jussi Eloranta[3]
[1]*Dipartimento di Fisica e Astronomia "Galileo Galilei" and CNISM, Università di Padova, via Marzolo 8, 35122 Padova, Italy and CNR-IOM Democritos, via Bonomea, 265–34136 Trieste, Italy*
[2]*Department of Physics and Astronomy, California State University, Northridge, Northridge, California 91330, USA*
[3]*Department of Chemistry and Biochemistry, California State University, Northridge, Northridge, California 91330, USA*

(Received 2 June 2017; revised manuscript received 21 September 2017; published 18 January 2018)

The existence of bright solitons in bulk superfluid ^{4}He is demonstrated by time-resolved shadowgraph imaging experiments and density functional theory (DFT) calculations. The initial liquid compression that leads to the creation of nonlinear waves is produced by rapidly expanding plasma from laser ablation. After the leading dissipative period, these waves transform into bright solitons, which exhibit three characteristic features: dispersionless propagation, negligible interaction in a two-wave collision, and direct dependence between soliton amplitude and the propagation velocity. The experimental observations are supported by DFT calculations, which show rapid evolution of the initially compressed liquid into bright solitons. At high amplitudes, solitons become unstable and break down into dispersive shock waves.

DOI: 10.1103/PhysRevLett.120.035302

Solitons are localized nonlinear waves in a medium, which do not disperse as a function of time and exhibit no interaction during a two-wave collision. After their discovery in the early 1800s, solitons have been observed in many different media, which exhibit pronounced nonlinear response. In recent years, solitons have become an intense field of research due to their important applications in areas such as plasma physics, electronics, biology, and optics [1]. Mathematical description of solitons can be formulated in terms of model dependent nonlinear partial differential equations (e.g., the nonlinear Schrödinger equation). In general, it has been established that nonlinear excitations (i.e., shock waves and solitons) exhibit distinct dependency between their amplitude and propagation velocity [1].

Solitons in thin ^{4}He films adsorbed on solid substrates have been studied extensively by both experiments [2–5] and theory [6–9]. The film thickness is typically only a few atomic layers, which supports the propagation of third sound [10]. When the film is driven by a sufficiently large amplitude excitation, the response of the system becomes nonlinear and typically follows the Korteweg–de Vries (KdV) equation [4,7]. The KdV equation is known to support solitonic solutions, which have been confirmed experimentally for helium films in the previously mentioned references. Solitons have also been observed experimentally in related systems such as Bose-Einstein condensates (BECs) and ^{3}He (magnetic solitons) [11–20]. In the former case, experimental observations have been successfully modeled by the Gross-Pitaevskii (GP) equation [21–23]. However, bright solitons have not been observed in bulk superfluid ^{4}He up to date. Such observation would not only provide important details of the underlying nonlinear response of this quantum liquid, but it would also allow for the study of soliton dynamics (including dissipation) over much longer propagation distances and times than currently possible in BECs.

Studies of nonlinear excitations in bulk superfluid helium are scarce. Most experiments have concentrated on the propagation of second sound shock waves [24–26] whereas nonlinear first sound has received very little attention. In the latter case, the efforts have mainly concentrated on the construction of cryogenic compression shock tubes [27–29], which can be used to generate shock waves in the liquid and study their properties (e.g., velocity, amplitude). Shock waves, unlike solitons, are known to exhibit strong dissipation and dispersion [30]. Semiempirical analysis of shock waves can be carried out by the Rankine-Hugoniot theory or its extension that is applicable in the superfluid phase [31]. As shown in a recent study, shock waves in superfluid helium evolve on a nanosecond time scale and hence time-resolved experiments are required for their characterization [32].

Because of the lack of sufficiently accurate theoretical models for bulk superfluid helium, the possible existence of solitons and their properties in this medium have not been studied previously. Note that neither GP or KdV equations are applicable for superfluid helium. Only nonlocal phenomenological models, such as density functional theory (DFT) [33,34], can describe the atomic-scale static and dynamic response of superfluid helium accurately. While previous time-dependent DFT (TDDFT) calculations have noted the existence of supersonic nonlinear waves [35,36], their nature and properties were not studied further. Consequently, no experimental efforts have been put forward to prove (or disprove) the existence of solitons in this medium. The obvious differences between helium

 © 2018 American Physical Society

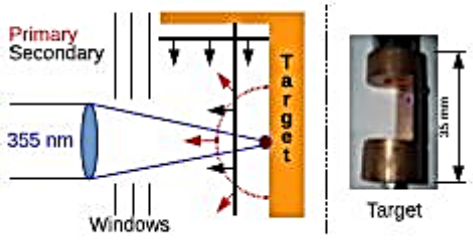

FIG. 1. Metal target geometry (scale accuracy ± 10 μm). The primary waves (red) originate from the expanding plasma created by laser ablation (red circle) whereas the planar waves (black) are created by rapid boiling on the target surface. The optical axis for imaging is perpendicular to the plane shown. A photograph of the target is shown on the right.

films and the bulk liquid are the dimensionality (2D vs 3D) and the presence of the film supporting substrate. The latter influences the sound velocity as a function of depth, which makes the application of a KdV-type equation attractive [37].

In this work, we report on the first experimental observation of bright solitons in bulk superfluid ^{4}He, which are created by rapidly expanding plasma and boiling on a metal target surface. In addition to the experimental evidence, their existence and dynamic properties are also studied by TDDFT.

The experiments employed a focused (spot diam. 50 μm) laser pulse (3rd harmonic 355 nm; 9 ns pulse length; 0.5 GW/cm^2; Continuum Minilite-II Nd-YAG laser) to generate plasma on the surface of a solid copper target immersed in bulk superfluid helium between 1.7 and 2.1 K at saturated vapor pressure (Oxford Variox or Janis 8DT cryostat) [32]. A schematic target configuration is depicted in Fig. 1. The initial radial plasma expansion [38–40] leads to nonlinear excitation of the surrounding liquid, which was visualized by time-resolved shadowgraph photography using a monochrome charge-coupled device (CCD; Imaging Source DMK23U445) equipped with 180X zoom lens (working dist. 95 mm; max. resol. 1.7 μm/pixel and

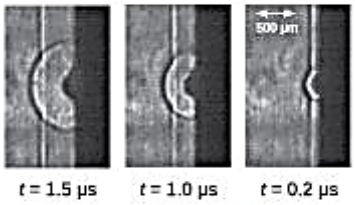

FIG. 2. Snapshots of the waves emitted from the target at given times t ($T = 1.7$ K). To increase the contrast in the images for display purposes, the lens system was placed slightly out of focus. The top portion of the target depicted in Fig. 1 is not shown.

focal depth ± 100 μm) and a delayed laser pulse (2nd harmonic 532 nm; 9 ns pulse length; Continuum Surelite-II Nd-YAG laser) as the background light. The contrast in the images is given by the Laplacian of the liquid density, which identifies the propagating wave edges. Because of scattering of the backlight, the images also show some contrast inside the wave.

A closeup of the system at early times is shown in Fig. 2. The primary wave emission is produced directly by the expanding plasma (half-spherical geometry) whereas the secondary planar wave originates from boiling of liquid helium on the target surface and the subsequent rapid gas expansion. The latter process is a consequence of the fast heat transfer on the metal surface (propagation velocity up to 10^5 m/s) following the ablation event. In the long-time regime, both the primary half-spherical (width ~ 15 μm) and secondary planar waves propagate in superfluid helium without dispersion (rate < 0.025 m/s) until they disappear from the observation window after 10 mm. This behavior is consistent with solitons.

The time evolution of normalized shadowgraph intensity difference in front of the soliton vs immediately behind is shown in the bottom panel of Fig. 3. Assuming that the nature of the leftover liquid excitations (i.e., spatial variations in liquid density) does not evolve in time, this difference reflects the wave dissipation rate [41]. During the first ~ 3 μs, rapid dissipation of both spherical and planar solitons takes place along with the associated

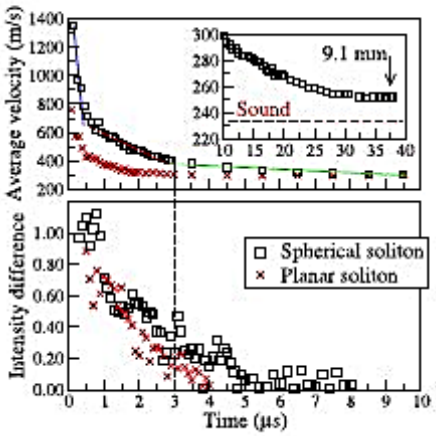

FIG. 3. The top panel shows the time evolution of the average soliton velocity (accuracy better than ± 1 m/s at long times) at 1.7 K with the long-time regime magnified in the inset (total travel distance indicated by an arrow). The three lines (blue, red, green) highlight the changes in the wave deceleration. The time axis refers to the delay between the ablation and backlight laser pulses. The bottom panel shows the normalized shadowgraph intensity difference in front of the wave vs behind it. The dashed line provides a guide to the eye for correlating the velocity and intensity difference data.

decrease in their propagation velocity (top panel of Fig. 3). The second regime ($t > 3\ \mu$s) exhibits a lower wave dissipation rate and the decrease in wave velocity begins to level off. As shown in the inset, the long-time ($t > 30\ \mu$s) soliton propagation appears nearly dissipationless as the velocity remains constant at slightly above the speed of first sound (instantaneous velocity ~250 m/s; see Ref. [32]). This limiting velocity follows the same temperature dependence as the first sound. We attribute the fast initial dissipation and reduction in the propagation velocity to a wave crest breaking process where the high density liquid is left behind as shocks. Note that a small decay in the velocity is also expected due to the finite viscosity present in the experiments [6] and the change in volume of the spherical soliton with increasing radius.

Another inherent property of solitons is that they emerge from a two-wave collision without any apparent change to their shape (apart from a possible change in phase). Collision between two solitons is shown in Fig. 4, where the primary half-spherical wave collides with the planar wave originated from the top section of the target. Because of the geometry of the emitted waves (half sphere vs plane), the two waves must intersect at the focal plane of the imagining system. The shadowgraph images clearly show that the solitons do not interact and continue to propagate unchanged after the collision. Furthermore, collision of the solitons with a metal surface (not shown) leads to effective reflection, but this is accompanied by energy loss as evidenced by an audible mechanical shock emitted into the metal. In the long-time regime, the reflected solitons from the cryostat walls can be observed to reach the target region again (total travel dist. 10 cm).

In addition to the experimental observations discussed above, we have also carried out TDDFT calculations in 3D [42] to identify solitonic solutions in bulk superfluid ^{4}He and study their dynamic properties. Within this model, helium is described by a complex valued order parameter

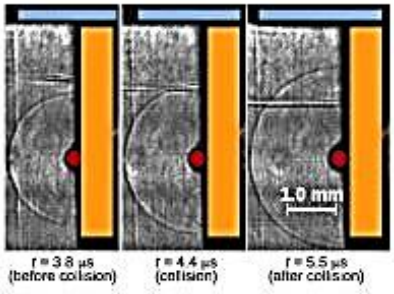

FIG. 4. Time evolution of the primary (spherical) and secondary (planar from top) solitons before, during, and after the collision ($T = 1.7$ K). The red circle indicates the origin for the primary wave emission and the top (blue) surface for the secondary wave. The delay between the ablation and backlight laser pulses is indicated by t.

$\Psi(\mathbf{r}, t)$, which is related to the atomic density as $\rho(\mathbf{r}, t) = |\Psi(\mathbf{r}, t)|^2$. The TDDFT equation is

$$i\hbar \frac{\partial}{\partial t}\Psi(\mathbf{r}, t) = \left(-\frac{\hbar^2}{2m}\nabla^2 + \frac{\delta \mathcal{E}_c}{\delta \rho}\right)\Psi(\mathbf{r}, t), \quad (1)$$

where m is the mass of ^{4}He and the functional $\mathcal{E}_c[\rho]$ was taken from Ref. [34]. This functional includes both finite-range and nonlocal corrections that are required to describe the $T = 0$ response of liquid ^{4}He accurately on the angstrom scale. Note that this model does not include viscous dissipation and cannot be propagated over long times (microseconds) due to limitations in current computational resources. For this reason, TDDFT cannot be used to study the related dissipative effects observed in the experiments. Furthermore, the accessible length scale is also very different from the experiments (i.e., nm vs μm). However, as discussed below, the TDDFT results can be scaled up to match the experiments.

To mimic the initial condition in the experiments (i.e., sudden compression by expanding plasma), the initial order parameter, $\Psi(\mathbf{r}, 0) = \sqrt{\rho(\mathbf{r}, 0)}$, is constructed as

$$\rho(\mathbf{r}, 0) = \rho_0[1 + (\Delta\rho/\rho_0)\sin^2(\pi x/\lambda_c)\Theta_w(x)], \quad (2)$$

where Θ_w represents a "box function" centered at x_0 with width $w = n\lambda_c$ (with n integer), i.e., $\Theta_w(x) = 1$ when $x_0 - w/2 < x < x_0 + w/2$ and $\Theta_w = 0$ otherwise. Equation (2) represents a square profile with average value $\Delta\rho/2$ that is superimposed on uniform bulk density ρ_0 (0.0218 Å^{-3} at $T = 0$) and modulated along the x axis with wavelength $\lambda_c = 3.58$ Å. This ansatz is based on the following assumptions: (i) when the liquid is rapidly compressed, the local density is increased with respect to the bulk and (ii) liquid ^{4}He flowing at a velocity greater than the Landau critical velocity (v_L) undergoes a transition from a spatially homogeneous liquid to a layered state characterized by a periodic density modulation along the direction of propagation (wavelength λ_c and amplitude determined by $v - v_L$) [43,44]. Such layered structures with densities higher than the bulk have also been observed in DFT simulations of fast moving particles in liquid ^{4}He [45].

During the early stages of the time evolution of $\rho(\mathbf{r}, t)$, dispersive low-amplitude supersonic waves with wavelength $\sim\lambda_c$ were produced (not shown). For the sake of clarity, we show smoothed density profiles after taking a local average of the density within a space window of $\pm 2\lambda_c$. We wish to stress that this procedure is just postprocessing and therefore it does not affect the time evolution itself. Note that the applied theoretical model must be able to describe the underlying atomic scale internal structure of the soliton.

When the initial state given by Eq. (2) is propagated in time using Eq. (1), it splits rapidly into two counterpropagating bright solitons as shown in Fig. 5. In contrast,

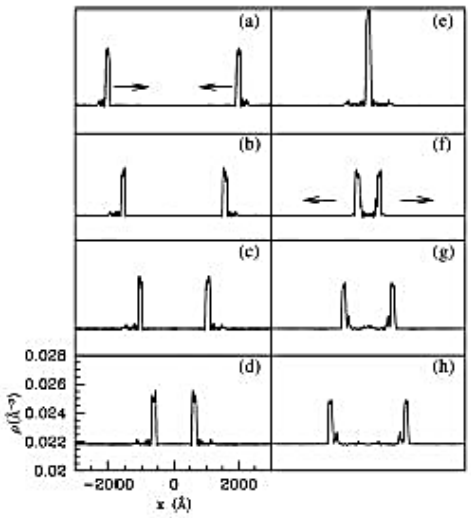

FIG. 5. Snapshots of superfluid ^{4}He density along the direction of soliton propagation (x axis) from TDDFT. The initial compression was created on the simulation box boundary with $n = 30$ (see text). Because of the periodic boundary condition, the solitons propagate as shown in (a)–(d), collide in (e), and continue propagating almost unchanged in (f)–(h). When compared with experiments, the x axis is oriented perpendicular to the ablation target.

due to the presence of the expanding plasma and the target in the experiments, only one soliton may form following the initial compression. The initial position x_0 of the square profile was placed at the simulation box boundary and, due to the periodic boundary condition, the two solitons resulting from the initial splitting move away from the boundaries towards the center. Note that the soliton width (~20 nm for the case shown) and height are well preserved during the time evolution. In comparison, a Gaussian wave packet with the same width and amplitude would disperse rapidly at 90 m/s. The solitons were also found to be stable with respect to random distortions introduced into the order parameter.

The relationship between the average soliton height ρ_s, which is controlled by the value of $\Delta\rho/\rho_0$ in Eq. (2), and its propagation velocity exhibits nearly linear behavior at low amplitudes as shown in Fig. 6. In the limit of very small amplitudes, the velocity approaches the speed of sound. When the amplitude ρ_s/ρ_0 is increased above 1.3, the system becomes unstable and evolves rapidly into a series of shock waves. This instability may be related to the previously mentioned wave crest breaking phenomenon, which was observed before 3 μs in Fig. 3. The calculated maximum stable soliton velocity (~430 m/s) corresponds approximately to the point where the rapid velocity decay levels off (dashed line near 3 μs in Fig. 3). The long-time

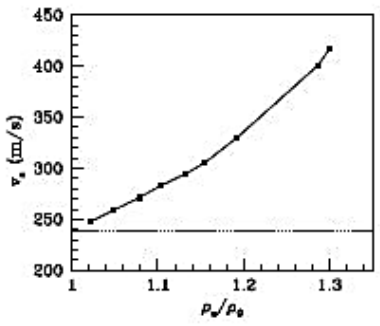

FIG. 6. Soliton propagation velocity (v_s) vs amplitude (ρ_s/ρ_0) from TDDFT. The horizontal dotted line indicates the velocity of first sound in superfluid ^{4}He at $T = 0$.

wave propagation velocity in the experiments remained slightly above the speed of sound, which corresponds to ~3% density increase at the soliton with respect to the bulk liquid (cf. Figs. 3 and 6). Both the lack of dispersion and the distinct amplitude-velocity dependence are characteristic to solitons.

When the initial width of the compression in Eq. (2) is increased, the width of the emitted solitons increases accordingly. Therefore, despite the obvious difference in the length scale between TDDFT and the experiments, this suggests that the presented nanometer-scale mechanism can scale up to micrometers. We also note that the presented solitonic waves from Eq. (2) can only be observed using a finite-range nonlocal energy density functional whereas local models, such as GP fitted to reproduce the speed of sound, do not support such solutions.

A collision between two solitons from TDDFT is shown in Fig. 5. Based on the simulations, the amplitude, shape, and velocity of the solitons are well preserved after the collision. This observation is in agreement with the experimental images shown in Fig. 4. At the point of collision shown in panel (e), the solitons interfere constructively as they both have a common phase factor (i.e., identical origin). If a soliton is made to collide with an exponentially repulsive wall (not shown), TDDFT calculations show that it loses its shape partially and dissipates some of the energy as shock waves. This behavior is also consistent with the experimental observations.

In summary, we have shown for the first time that bulk superfluid ^{4}He can support bright solitonic waves. This is evidenced by both direct experimental observations as well as theoretical modeling based on TDDFT. The liquid compression created by the expanding plasma is sufficiently high such that the resulting nonlinear response can counteract the dispersive effects. This is in contrast to previously studied thin liquid helium films where the presence of the supporting substrate played a major role in producing the necessary nonlinear response. In bulk

superfluid helium, solitons become unstable when their amplitude exceeds a critical threshold, which corresponds to a velocity slightly above 400 m/s.

This work was supported by National Science Foundation Grant No. DMR-1205734. The authors thank M. Barranco, M. Pi, and L. Salasnich for helpful discussions.

[1] P. G. Drazin and R. S. Johnson, *Solitons: An Introduction*, Cambridge Texts in Applied Mathematics, 2nd ed. (Cambridge University Press, Cambridge, England, 1989).
[2] K. Kono, S. Kobayashi, and W. Sasaki, J. Phys. Soc. Jpn. **50**, 721 (1981).
[3] V. A. Hopkins, J. Keat, G. D. Meegan, T. Zhang, and J. D. Maynard, Phys. Rev. Lett. **76**, 1102 (1996).
[4] M. J. McKenna, R. J. Stanley, E. DiMasi, and J. D. Maynard, Physica (Amsterdam) **165B–166B**, 603 (1990).
[5] A. A. Levchenko, G. V. Kolmakov, L. P. Mezhov-Deglin, and V. B. Shikin, JETP Lett. **65**, 572 (1997).
[6] B. A. Huberman, Phys. Rev. Lett. **41**, 1389 (1978).
[7] S. Nakajima, S. Kurihara, and K. Tohdoh, J. Low Temp. Phys. **39**, 465 (1980).
[8] A. C. Biswas and C. S. Warke, Phys. Rev. B **28**, 6539 (1983).
[9] R. Balakrishnan, Phys. Rev. B **42**, 6153 (1990).
[10] K. R. Atkins, Phys. Rev. **113**, 962 (1959).
[11] S. Burger, K. Bongs, S. Dettmer, W. Ertmer, K. Sengstock, A. Sanpera, G. V. Shlyapnikov, and M. Lewenstein, Phys. Rev. Lett. **83**, 5198 (1999).
[12] J. Denschlag, J. E. Simsarian, D. L. Feder, C. W. Clark, L. A. Collins, J. Cubizolles, L. Deng, E. W. Hagley, K. Helmerson, W. P. Reinhardt, S. L. Rolston, B. I. Schneider, and W. D. Phillips, Science **287**, 97 (2000).
[13] B. P. Anderson, P. C. Haljan, C. A. Regal, D. L. Feder, L. A. Collins, C. W. Clark, and E. A. Cornell, Phys. Rev. Lett. **86**, 2926 (2001).
[14] L. Khaykovich, F. Schreck, G. Ferrari, T. Bourdel, J. Cubizolles, L. D. Carr, Y. Castin, and C. Salomon, Science **296**, 1290 (2002).
[15] G. B. Partridge, A. G. Truscott, and R. G. Hulet, Nature (London) **417**, 150 (2002).
[16] J. H. V. Nguyen, D. Luo, and R. G. Hulet, Science **356**, 422 (2017).
[17] A. L. Marchant, T. P. Billiam, T. P. Wiles, M. M. H. Yu, S. A. Gardiner, and S. L. Cornish, Nat. Commun. **4**, 1865 (2013).
[18] C. M. Gould and D. M. Lee, Phys. Rev. Lett. **37**, 1223 (1976).
[19] K. Maki and P. Kumar, Phys. Rev. Lett. **38**, 557 (1977).
[20] V. P. Mineyev and G. E. Volovik, Phys. Rev. B **18**, 3197 (1978).
[21] F. Kh. Abdullaev and J. Garnier, *Bright Solitons in Bose-Einstein Condensates: Theory in Emergent Non-Linear Phenomena in Bose-Einstein Condensates*, Atomic, Optical, and Plasma Physics (Springer, New York, 2008).
[22] C. Hamner, J. J. Chang, P. Engels, and M. A. Hoefer, Phys. Rev. Lett. **106**, 065302 (2011).
[23] D. K. Efimkin, J. Hofmann, and V. Galitski, Phys. Rev. Lett. **116**, 225301 (2016).
[24] D. V. Osborne, Proc. Phys. Soc. London Sect. A **64**, 114 (1951).
[25] A. Yu. Iznankin and L. P. Mezhov-Deglin, Sov. Phys. JETP **57**, 801 (1983).
[26] R. J. Atkin and N. Fox, J. Phys. C **18**, 1585 (1985).
[27] J. C. Cummings, J. Fluid Mech. **75**, 373 (1976).
[28] W. J. Nellis, N. C. Holmes, A. C. Mitchell, R. J. Trainor, G. K. Governo, M. Ross, and D. A. Young, Phys. Rev. Lett. **53**, 1248 (1984).
[29] H. Nagai, Ph.D. thesis, University of Tsukuba, 2000.
[30] M. Remoissenet, *Waves Called Solitons*, Advanced Texts in Physics, 3rd ed. (Springer, New York, 2003).
[31] D. M. Moody and B. Sturtevant, Phys. Fluids **27**, 1125 (1984).
[32] A. Garcia, X. Buelna, E. Popov, and J. Eloranta, J. Chem. Phys. **145**, 124504 (2016).
[33] F. Dalfovo, A. Lastri, L. Pricaupenko, S. Stringari, and J. Treiner, Phys. Rev. B **52**, 1193 (1995).
[34] F. Ancilotto, M. Barranco, F. Caupin, R. Mayol, and M. Pi, Phys. Rev. B **72**, 214522 (2005).
[35] J. Eloranta and V. A. Apkarian, J. Chem. Phys. **117**, 10139 (2002).
[36] A. Hernando, M. Barranco, M. Pi, Marti, E. Loginov, M. Langlet, and M. Drabbels, Phys. Chem. Chem. Phys. **14**, 3996 (2012).
[37] S. Nakajima, K. Todoh, and S. Kurihara, J. Low Temp. Phys. **41**, 521 (1980).
[38] X. Buelna, E. Popov, and J. Eloranta, J. Low Temp. Phys. **186**, 197 (2017).
[39] X. Buelna, A. Freund, D. Gonzalez, E. Popov, and J. Eloranta, J. Phys. Chem. B **120**, 11010 (2016).
[40] K. Sasaki and N. Takada, Pure Appl. Chem. **82**, 1317 (2010).
[41] G. S. Settles, *Schlieren and Shadowgraph Techniques* (Springer, New York, 2006).
[42] F. Ancilotto, M. Barranco, F. Coppens, J. Eloranta, N. Halberstadt, A. Hernando, D. Mateo, and M. Pi, Int. Rev. Phys. Chem. **36**, 621 (2017).
[43] L. P. Pitaevskii, JETP Lett. **39**, 511 (1984).
[44] F. Ancilotto, F. Dalfovo, L. P. Pitaevskii, and F. Toigo, Phys. Rev. B **71**, 104530 (2005).
[45] F. Ancilotto, M. Barranco, J. Eloranta, and M. Pi, Phys. Rev. B **96**, 064503 (2017).